

Prevalent externally-driven protoplanetary disc dispersal as a function of the galactic environment

Andrew J. Winter,^{1,2,3}★ J. M. Diederik Kruijssen,¹ Mélanie Chevance,¹
Benjamin W. Keller,¹ Steven N. Longmore⁴

¹*Astronomisches Rechen-Institut, Zentrum für Astronomie der Universität Heidelberg, Mönchhofstraße 12-14, 69120 Heidelberg, Germany*

²*Institute of Astronomy, University of Cambridge, Madingley Road, Cambridge CB3 0HA, UK*

³*Department of Physics and Astronomy, University of Leicester, Leicester, LE1 7RH, UK*

⁴*Astrophysics Research Institute, Liverpool John Moores University, IC2, Liverpool Science Park, 146 Brownlow Hill, Liverpool L3 5RF, UK*

Accepted 2019 September 27; Received 2019 September 23; in original form 2019 July 4

ABSTRACT

The stellar birth environment can significantly shorten protoplanetary disc (PPD) lifetimes due to the influence of stellar feedback mechanisms. The degree to which these mechanisms suppress the time and mass available for planet formation is dependent on the local far-ultraviolet (FUV) field strength, stellar density, and ISM properties. In this work, we present the first theoretical framework quantifying the distribution of PPD dispersal time-scales as a function of parameters that describe the galactic environment. We calculate the probability density function for FUV flux and stellar density in the solar neighbourhood. In agreement with previous studies, we find that external photoevaporation is the dominant environment-related factor influencing local stellar populations after the embedded phase. Applying our general prescription to the Central Molecular Zone of the Milky Way (i.e. the central ~ 250 pc), we predict that 90% of PPDs in the region are destroyed within 1 Myr of the dispersal of the parent molecular cloud. Even in such dense environments, we find that external photoevaporation is the dominant disc depletion mechanism over dynamical encounters between stars. PPDs around low-mass stars are particularly sensitive to FUV-induced mass loss, due to a shallower gravitational potential. For stars of mass $\sim 1 M_{\odot}$, the solar neighbourhood lies at approximately the highest gas surface density for which PPD dispersal is still relatively unaffected by external FUV photons, with a median PPD dispersal timescale of ~ 4 Myr. We highlight the key questions to be addressed to further contextualise the significance of the local galactic environment for planet formation.

Key words: planets and satellites: formation — protoplanetary discs — stars: formation — galaxies: ISM — galaxies: star clusters: general — galaxies: star formation

1 INTRODUCTION

The process of planet formation is strongly dependent on the stellar birth environment. The majority of stars exist in clusters or associations within their first few Myr of evolution (Lada & Lada 2003; Longmore et al. 2014; Krumholz et al. 2019), during which time they also host protoplanetary discs (PPDs - e.g. Haisch et al. 2001; Ribas et al. 2014). Multiple feedback mechanisms influence disc evolution. In sufficiently dense environments, star-disc encounters can truncate the disc and induce increased accretion rates (Clarke & Pringle 1993; Ostriker 1994; Hall et al. 1996; Pfalzner et al. 2005a; Olczak et al. 2006; Pfalzner et al. 2006; de Juan Ovelar et al. 2012; Breslau et al. 2014; Rosotti et al. 2014; Winter et al. 2018a). Recent studies indicate that in the solar

neighbourhood such interactions only have a significant effect in the early stages of cluster evolution due to enhanced stellar multiplicity and substructure, and therefore set initial conditions rather than destruction time-scales (Winter et al. 2018b,c; Bate 2018). However, in regions with massive stars, external photoevaporation by far-ultraviolet (FUV) and extreme-ultraviolet (EUV) photons can rapidly disperse PPDs (Johnstone et al. 1998; Störzer & Hollenbach 1999; Armitage 2000; Clarke 2007; Fatuzzo & Adams 2008; Adams 2010; Facchini et al. 2016; Ansdell et al. 2017; Haworth et al. 2018b; Winter et al. 2018b). Additionally, before the dispersal of the parent giant molecular cloud (GMC), ram pressure stripping can truncate PPDs (Wijnen et al. 2017a) or additional material can be accreted (Moeckel & Throop 2009; Scicluna et al. 2014), leading to the destruction and reforming of discs during the embedded phase (Bate 2018). If a PPD is destroyed quickly by feedback in dense stellar envi-

★ ajwinter@ast.cam.ac.uk

ronments, planets may be unable to form, depending on the efficiency of the formation mechanisms (Youdin & Goodman 2005; Johansen & Lambrechts 2017; Ormel et al. 2017; Haworth et al. 2018a). Given the apparent ubiquity of grouped star formation, quantifying the destruction time-scales for PPDs due to neighbour feedback is of great relevance for understanding the demographics of PPDs and exoplanetary systems.

Although stars are understood to form primarily in groups, the nature of those groups is diverse and remains the topic of debate; however, it is evident that a density continuum well describes the distribution of the interstellar medium (Vazquez-Semadeni 1994; Padoan & Nordlund 2002; Hill et al. 2012) and stars (Bressert et al. 2010; Kruijssen 2012). Previous statistical investigations into PPD destruction by stellar feedback have been focused on young star-forming environments in the solar neighbourhood ($\lesssim 1$ – 2 kpc from the Sun, e.g. Fatuzzo & Adams 2008). However, this approach may not yield a representative picture, since star and planet formation in the Milky Way historically proceeded at much greater gas densities, similar to those seen near the galactic centre (Kruijssen & Longmore 2013).

Recent work shows that the properties of GMCs and young stellar clusters depend on the galactic-scale interstellar medium (ISM) properties (e.g. Bolatto et al. 2008; Heyer et al. 2009; Longmore et al. 2014; Adamo et al. 2015; Freeman et al. 2017; Reina-Campos & Kruijssen 2017; Sun et al. 2018). For example, the density threshold required for star formation to proceed is at least an order of magnitude higher in the central ~ 250 pc of the Milky Way (the Central Molecular Zone; CMZ) than in the solar neighbourhood (Longmore et al. 2013; Kruijssen et al. 2014; Rathborne et al. 2014; Ginsburg et al. 2018). Given that at higher densities, star-disc encounters are more frequent and FUV fields are stronger (Winter et al. 2018b), we would expect PPD lifetimes to be reduced in the CMZ with respect to the galactic disc. Indeed, preliminary studies into the PPD population towards the CMZ indicate low disc survival fractions in young stellar populations (Stolte et al. 2010, 2015).

Due to the above considerations, this work is aimed at linking PPD lifetimes to the distribution of molecular gas from which the stellar populations form, thereby establishing time-scales available for planet formation as a function of quantities describing the local galactic environment. We will primarily consider the influence of FUV-induced mass loss, which Winter et al. (2018b) demonstrates to dominate over dynamical encounters in observed environments.¹ This represents a generalisation of the study of Fatuzzo & Adams (2008), where only local star-forming environments were considered. The present study also incorporates other recent advances in our understanding of GMC properties and clustered star formation. Due to recent developments in the theory of FUV-induced PPD mass loss rates (Facchini et al. 2016; Haworth et al. 2018b), we are additionally able to estimate the time-scales for PPD destruction based on the properties of the disc and the mass of its host star.

In this paper, we first review the time-scales for PPD

dispersal as a result of environmental influences in Section 2. We then characterise the stellar birth environment by establishing probability density functions (PDFs) in stellar density–FUV flux space as a function of the average gas properties in the solar neighbourhood and the CMZ (Section 3). For the reader interested only in our main results, Section 4 discusses PPD lifetimes as a function of large scale ISM properties. We present our concluding remarks in Section 5.

2 PPD DESTRUCTION TIME-SCALES

2.1 External photoevaporation

In this section, we will establish characteristic time-scales for PPD destruction due to FUV irradiation. We will henceforth disregard the mass loss of PPDs due to EUV flux because photons in that energy range only dominate mass loss at extremely small ($\ll 0.1$ pc) and large ($\gg 10$ pc) spatial separations from massive stars (although these numbers depend on disc properties and the irradiating source – Störzer & Hollenbach 1999; Winter et al. 2018b). In this case, time-scales for disc dispersal by external photoevaporation are either rapid ($\ll 1$ Myr) or slow ($\gg 3$ Myr) respectively. For rapid dispersal we are less interested in establishing the exact time at which PPDs are destroyed, and more in the prediction that they are sufficiently short-lived such that planet formation is likely suppressed or significantly influenced. For discs where the FUV-induced mass loss is small, PPD depletion is dictated by internal processes such as internal photoevaporation and accretion. We therefore limit our attention to the influence of FUV photons in the following discussion. Henceforth we will refer to the flux F and luminosity L without subscripts for simplicity; it is to be understood that we refer only to the contribution of the FUV photons.

We will now calculate the FUV-induced PPD destruction time-scale τ_{FUV} as a function of FUV flux F , host mass m_* and viscous time-scale τ_{visc} . Each of these parameters has a significant impact on survival time-scales. FUV mass loss rates increase with F for $F \lesssim 10^4 G_0$; above this threshold the temperature of the photodissociation region is a weak function of F , and therefore so too is the mass flux in the thermal wind (e.g. Tielens & Hollenbach 1985; Hollenbach & Tielens 1997; Johnstone et al. 1998). The efficiency of FUV-induced mass loss increases with decreasing stellar host mass simply due to a shallower gravitational potential, and therefore lower escape velocity. Finally, the time-scale for viscous spreading is important since this dictates the rate at which material is accreted onto the central star, and the dispersal time-scale once the reservoir of material in outer disc has been depleted (see Clarke et al. 2001, for a discussion in the context of internal photoevaporation). For the rate of mass loss carried in the thermal wind \dot{M}_{wind} , we apply the FRIED grid (Haworth et al. 2018b) for a given outer disc radius R_d , disc mass M_d , F and m_* . This is combined with a viscous disc evolution model, discussed below, to calculate PPD destruction time-scales.

¹ As discussed previously, ram pressure stripping and dynamical encounters can also alter disc evolution, and they are further discussed in Section 2.

2.1.1 Viscous disc evolution model

We calculate the one-dimensional viscous disc evolution using the method of [Clarke \(2007\)](#), and subsequently [Anderson et al. 2013](#); [Rosotti et al. 2017](#); [Winter et al. 2018b](#)). In such a parametrization, viscosity is assumed to scale linearly with radius r within the disc, which corresponds to a temperature profile which scales with $r^{-1/2}$ and a constant α -viscosity parameter ([Shakura & Sunyaev 1973](#)). Conveniently, this prescription has similarity solutions for the disc evolution ([Lynden-Bell & Pringle 1974](#)). For a viscosity which is proportional to r , such a solution for the surface density profile of the disc has the form:

$$\Sigma_d = \frac{M_{d,0}}{2\pi R_1^2 \eta} \exp\left(-\frac{\eta}{T}\right) T^{-1.5} \quad (1)$$

where $M_{d,0}$ is the initial disc mass, $\eta \equiv r/R_1$ with R_1 the initial disc scaling radius, and $T = 1 + t/\tau_{\text{visc}}$ for time t with τ_{visc} the viscous time-scale at R_1 . In quantifying the FUV induced destruction time-scale τ_{FUV} , we will vary τ_{visc} rather than the viscosity parameter α . These two quantities can be related by the expression:

$$\alpha \approx 5.4 \times 10^{-3} \left(\frac{\tau_{\text{visc}}}{\text{Myr}}\right)^{-1} \left(\frac{R_1}{40 \text{ au}}\right)^{3/2} \left(\frac{m_*}{M_\odot}\right)^{-1/2}. \quad (2)$$

Initially we truncate the surface density outside $R_{d,0} = 2.5R_1$ to ensure a well-defined outer radius. We further assume that the initial disc mass is $M_{d,0} = 0.1 m_*$ for all of our calculations (e.g. [Andrews et al. 2013](#); [Pascucci et al. 2016](#)).

Numerically, the evolving surface density is defined over a one-dimensional grid evenly spaced in $r^{1/2}$ in the range 0.5–800 au, with 500 cells. A zero torque boundary condition is applied at the inner edge, and the cell at the outer edge experiences a mass flux due to both the viscous outflow and the FUV-induced wind (with loss rate \dot{M}_{wind} obtained by interpolating over the FRIED grid – [Haworth et al. 2018b](#)). The outer edge evolves at each timestep depending on whether there is net mass loss or accumulation. We consider a disc to be ‘destroyed’ if $M_d < 10^{-5} M_\odot$, although our results are insensitive to this threshold since extremely low mass PPDs are quickly depleted by photoevaporation. If the disc survives for longer than 10 Myr, we assume that it is dispersed by internal processes, such that $\tau_{\text{FUV}} \leq 10$ Myr throughout the parameter space.

2.1.2 Fitting formula

We impose a simple fitting formula to PPD FUV-induced destruction time-scale:

$$\tau_{\text{FUV}} = \theta_0 \left(\frac{\tau_{\text{visc}}}{\text{Myr}}\right)^{\theta_1} \left(\frac{m_*}{M_\odot}\right)^{\theta_2} \left\{ \exp\left[-\left(\frac{F}{5 \cdot 10^3 G_0}\right)^{\theta_3}\right] + 1 \right\} \times \left[\left(\frac{F}{5 \cdot 10^3 G_0}\right)^{-\theta_4} + 1 \right] \text{ Myr}, \quad (3)$$

where $\theta_{0,1,2,3}$ are fitting parameters. In equation 3 we have imposed an effective minimum destruction time-scale for $F \gtrsim 10^4 G_0$. For $F \gtrsim 10^4 G_0$ the temperature in the photodissociation region ($\sim 10^4$ K) is insensitive to F and the mass flux in the thermal wind remains approximately constant as discussed above. We have also included an intermediate regime ($10^3 G_0 \lesssim F \lesssim 10^4 G_0$) where τ_{FUV} drops

	θ_0	θ_1	θ_2	θ_3	θ_4
θ_i	0.59	0.70	0.71	3.9	0.36
Associated var.	τ_{FUV}	τ_{visc}	m_*	F	F

Table 1. Table of fitting parameters for equation 3.

rapidly with increasing F ; here FUV driven winds dominate mass loss throughout the lifetime of the disc. At lower F , the power-law relationship is weaker since accretion rates are comparable to wind driven mass loss. Fitting this formula, we obtain the values summarised in Table 1. In Figure 1, the numerical calculations based on the one-dimensional viscous evolution models are compared with the analytic estimate from equation 3. The fitting formula reproduces the results to within a factor of order unity throughout the parameter space.

2.2 Dynamical encounters

The influence of dynamical encounters on PPD evolution has been investigated extensively (e.g. [Ostriker 1994](#); [Hall et al. 1996](#); [Pfalzner et al. 2005a](#); [Olczak et al. 2006](#); [Pfalzner et al. 2006](#); [Breslau et al. 2014](#); [Winter et al. 2018a](#)), and we do not expand upon the findings of those previous studies here. We instead use the result that multiple distant encounters have little effect on a disc in comparison to a single close encounter ([Ostriker 1994](#); [Winter et al. 2018a](#)). This means that we are free to limit our consideration to the time-scale on which one such close encounter occurs in a given environment. A consequence of this is that the tidal destruction time-scale is practically independent of the viscous evolution time-scale.

Following [Binney & Tremaine \(1987\)](#), see also [Ostriker 1994](#) we can relate the impact parameter b for a given encounter to the closest approach distance z_{min} :

$$b^2 = z_{\text{min}}^2 \left(1 + \frac{Gm_{\text{tot}}}{v_\infty^2 z_{\text{min}}} \right) \quad (4)$$

where the second term in the brackets corresponds to gravitational focusing and v_∞ is the relative velocity of the two stars at infinity. The total mass $m_{\text{tot}} = m_* + m_p$ is the sum of the host and the perturber mass. Integrating over a Boltzmann distribution for v_∞ , we can write the differential encounter rate:

$$d\mathcal{E} = \frac{2\sqrt{\pi} Gm_{\text{tot}} \rho_*}{\langle m_* \rangle \sigma_{v*}} \left(1 + \frac{4\sigma_{v*}^2 z_{\text{min}}}{Gm_{\text{tot}}} \right) \xi_*(m_p) dz_{\text{min}} dm_p, \quad (5)$$

where σ_{v*} is the local 1D stellar velocity dispersion and

$$\xi_*(m_*) \propto \begin{cases} m_*^{-1.3} & \text{for } 0.08 M_\odot \leq m_* < 0.5 M_\odot \\ m_*^{-2.3} & \text{for } 0.5 M_\odot \leq m_* < 100 M_\odot \\ 0 & \text{otherwise} \end{cases}, \quad (6)$$

is the [Kroupa \(2001\)](#) IMF, where $\xi_*(m_*)$ is normalised and continuous. Such an IMF gives a mean stellar mass $\langle m_* \rangle \approx 0.5 M_\odot$. For a fixed σ_{v*} , integrating equation 5 over the relevant range of z_{min} gives an overall encounter rate for en-

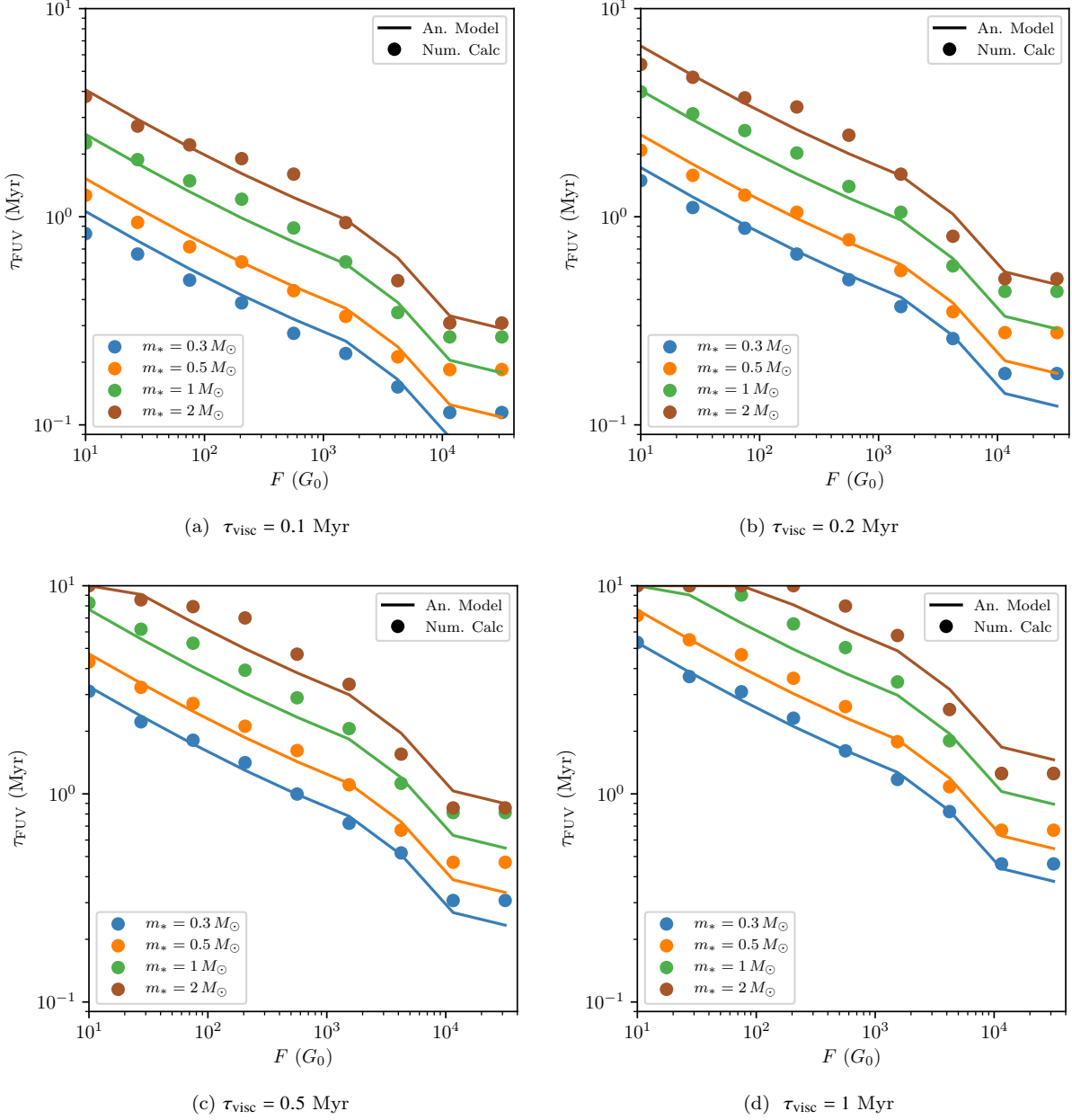


Figure 1. Time-scale for disc depletion due to FUV photons, τ_{FUV} for varying FUV flux F . Results are shown for different viscous time-scales τ_{visc} and stellar host masses m_* . Circular markers indicate the calculation using a viscous disc evolution model, while the lines are the value using our analytic fit (equation 3).

counters with closest approach distances smaller than \mathcal{Z}_{min} :

$$\frac{\partial \mathcal{E}}{\partial m_{\text{p},0}} = \frac{0.15 \rho_{*,4} \mathcal{Z}_{\text{min},2}}{\sigma_{v*,0}} \times \left(m_{*,0} + m_{\text{p},0} + 0.23 \mathcal{Z}_{\text{min},2} \sigma_{v*,0}^2 \right) \xi_*(m_{\text{p}}) \quad (7)$$

where

$$\rho_{*,4} \equiv \frac{\rho_*}{10^4 M_\odot \text{pc}^{-3}}; \sigma_{v*,0} \equiv \frac{\sigma_{v*}}{1 \text{ km/s}}; \mathcal{Z}_{\text{min},2} \equiv \frac{\mathcal{Z}_{\text{min}}}{100 \text{ au}}$$

and $m_{*,\text{p},0} \equiv m_{*,\text{p}}/1 M_\odot$.

The problem is now reduced to finding the appropriate value for \mathcal{Z}_{min} as a function of stellar mass. For a given encounter distance, the degree to which a disc is depleted also

depends on the orientation, mass ratio and eccentricity of the encounter (e.g. [Ostriker 1994](#); [Olczak et al. 2012](#); [Breslau et al. 2014](#); [Winter et al. 2018a,b](#)). Encounters are also more destructive if both stars host extended PPDs, where strongly interacting circumstellar material results in increased angular momentum exchange and disc mass loss (e.g. [Pfalzner et al. 2005b](#); [Muñoz et al. 2015](#)). However, a logical definition of a ‘destructive encounter’ is one after which the independently evolving disc does not survive long post-encounter. We introduce the gravitational radius (e.g. [Hollenbach et al.](#)

1994):

$$R_g = \frac{Gm_*}{c_s^2} = 8.9 \left(\frac{m_*}{1 M_\odot} \right) \text{ au}, \quad (8)$$

which is the radius at which photoionised gas is unbound from the stellar host ($c_s \sim 10$ km/s is the sound speed in ionised gas of temperature $\sim 10^4$ K). Internal photoevaporation drives thermal winds from R_g , resulting in a gap opening up at this radius and the quenching of viscous mass flow to the inner disc. [Clarke et al. \(2001\)](#) demonstrate that, after this gap opens, the short viscous time-scales at small radii lead to rapid dispersal of material inwards of R_g . Our threshold for a destructive encounter should therefore be one which plays the role of photoevaporative dispersal in that the encounter removes the majority of mass outwards of $\sim R_g$. For equal mass, parabolic, prograde star-disc encounters, this corresponds to $Z_{\min} \approx R_g/0.28$ au (e.g. [Breslau et al. 2014](#)). The separation required to induce significant angular momentum loss during a parabolic encounter scales with $(m_p/m_*)^{1/3}$ ([Winter et al. 2018a](#)), hence we have:

$$Z_{\min,2} = 0.31 m_{*,0}^{2/3} m_{p,0}^{1/3}. \quad (9)$$

Taking this upper limit in the closest approach distance and integrating equation 7 over m_p gives the encounter rate \mathcal{E} , or equivalently the tidal destruction time-scale:

$$\tau_{\text{tidal}} \equiv 1/\mathcal{E}. \quad (10)$$

The remaining free parameter is the local stellar velocity dispersion σ_{v*} , the dependence of τ_{tidal} on which is shown in Figure 2. Most star-forming regions have local $\sigma_{v*} \sim 2\text{--}10$ km/s, and τ_{tidal} varies by a factor of a few in this range. We choose a fiducial $\sigma_{v*} = 3$ km/s; the resulting value of τ_{tidal} is broadly consistent with previous findings that no significant truncation occurs for stellar number densities $\lesssim 10^4 \text{ pc}^{-3}$ (i.e. $\tau_{\text{tidal}} \gg 10$ Myr – see [Wijnen et al. 2017b; Winter et al. 2018b](#)), and that local stellar densities $> 10^5 \text{ pc}^{-3}$ are required for dynamical encounters to act as an efficient PPD dispersal mechanism ([Olczak et al. 2012; Vincke & Pfalzner 2018](#)). Our choice also means that, within a reasonable range for σ_{v*} , τ_{tidal} only varies by a factor of order a few. However, our evaluation of τ_{tidal} should be interpreted with caution since encounters are by their nature stochastic. Our estimate is intended as a guide as to the time-scale on which severely damaging encounters occur.

2.3 Ram pressure stripping

The influence of the interstellar medium is more complex to treat, since whether a PPD increases or decreases in mass is a function of both the local ISM density ρ_g and the ISM velocity with respect to a given host star \vec{v}_g ([Wijnen et al. 2017a](#)). Ultimately, realistic gas distributions can result in the destruction and reforming of a disc throughout the embedded phase ([Bate 2018](#)), and therefore discussion of time-scale for ram pressure induced disc destruction is inherently misleading. However, we can at least estimate a time-scale upon which the motion of a star through the ISM has a significant impact on the disc. This is approximately the time-scale on which the material accreted onto the disc approaches the mass of the disc itself. This can be written

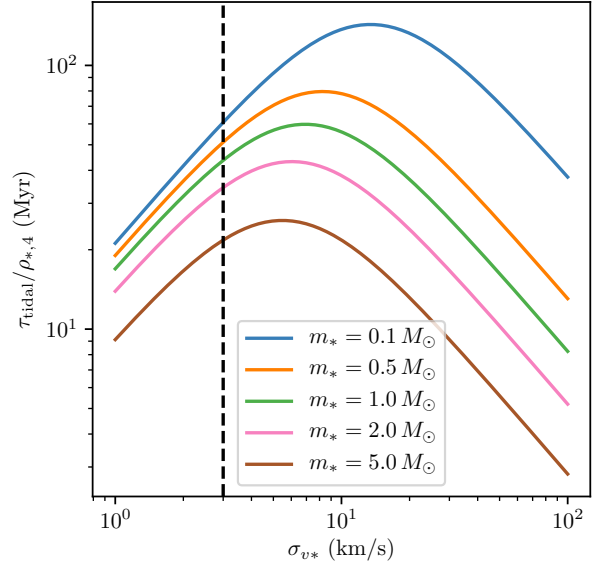


Figure 2. The encounter rate time-scale for stellar density $\rho_* = 10^4 M_\odot \text{ pc}^{-3}$ as a function of local velocity dispersion σ_{v*} . The dashed vertical line marks the adopted value of $\sigma_{v*} = 3$ km/s in our model.

([Wijnen et al. 2017a](#)):

$$\tau_{\text{ram}} \sim \frac{\Sigma_d}{5\rho_g v_g}, \quad (11)$$

where we will assume that $v_g = |\vec{v}_g| \approx 1$ km/s. By choosing the initial surface density close to R_1 , and assuming as before that $M_{d,0} = 0.1 m_*$, we can use equations 1 and 11 to estimate:

$$\tau_{\text{ram}} \sim \left(\frac{m_*}{M_\odot} \right) \left(\frac{\rho_g}{4 \times 10^4 M_\odot \text{ pc}^{-3}} \right)^{-1} \text{ Myr}. \quad (12)$$

This gas density threshold ($\rho_g \gtrsim 10^{-18} \text{ g cm}^{-3}$) for efficient ram pressure stripping of the PPD ($\tau_{\text{ram}} \lesssim 3$ Myr) is similar to that reported in [Wijnen et al. \(2017a\)](#). Since the response of a disc (accretion or depletion) to motion through a high gas density is uncertain, we will neglect further discussion of its influence on a PPD in this work.

2.4 Overall dispersal time-scale

We have now reviewed the time-scales on which three truncation processes act to deplete a PPD. Only dynamical encounters and external photoevaporation are necessarily dispersal mechanisms, and therefore when calculating the overall time for disc destruction we will focus on these two processes. For the total time-scale for PPD destruction by external influence, we therefore estimate the dispersal time-scale:

$$\tau_{\text{disp}} \approx \left(\tau_{\text{FUV}}^{-1} + \tau_{\text{tidal}}^{-1} \right)^{-1}, \quad (13)$$

where τ_{FUV} and τ_{tidal} are evaluated using equations 3 and 10, respectively. We are thus able to calculate contours of constant τ_{disp} in ρ_* - F space.

3 STELLAR BIRTH ENVIRONMENT

To calculate the distribution of FUV fluxes for a stellar population, [Fatuzzo & Adams \(2008\)](#) assumed a stellar density distribution based on observed star-forming regions within ~ 2 kpc and extended the sample to an assumed upper limit on the number of members $N = 10^5$ stars. Here we take a more general approach. We first relate the distribution of stellar densities to star formation physics, based on the theoretical arguments by [Kruijssen \(2012\)](#). This involves rewriting the lognormal gas density probability density function (PDF) in terms of the stellar overdensity in Section 3.1 and relating this to the properties of the galactic disc in Section 3.2. We then calculate the star formation efficiency (SFE) as a function of local gas density in Section 3.3. [Winter et al. \(2018b\)](#) demonstrate that the stellar density is related to local FUV flux in the limit of high mass regions, such that we can derive the PDF of the flux F from the stellar density PDF. To do this, we must also quantify the properties of neighbouring stars. The mass (and FUV luminosity) of the most massive local star decreases with decreasing mass of the star-forming region due to the stochastic sampling of the IMF, which we address in Section 3.4. This is related to FUV luminosity of the most massive member in Section 3.5. To obtain the fraction of stars born in a region of a certain mass, we consider the initial cluster mass function (ICMF – Section 3.6) as a function of galactic scale gas properties. We then quantify the statistical deviation from the ρ_* – F relationship that holds in the high-mass environment limit in Section 3.7, including an estimate of the FUV flux between star-forming regions. In this way, a combination of the ICMF and the stellar density PDF together determine the full, generalised 2D PDF for stellar birth environment in density–FUV space. The results of this process are presented in Section 3.8 for the solar neighbourhood and the CMZ.

Since stars form over a continuum of densities ([Bressert et al. 2010](#)), so far as is possible we will refrain from defining units of star formation (i.e. clusters/associations or GMCs). However, this definition will become necessary from Section 3.5, where we address the deviation from the ρ_* – F relationship. Some discussion of the definition of a ‘cluster’ is required. [Kruijssen \(2012\)](#) describes a model for the fraction of stellar clusters that remain bound, and therefore quantifies the initial bound fraction. However, we are only interested in the first few Myr of evolution; we are less concerned with whether or not a group of stars is a cluster or association. Henceforth, we will call all such groups ‘star-forming regions’ and neglect the influence of evaporation and expansion of the stellar population.

3.1 Stellar density PDF

Our first goal is to quantify the distribution of stellar densities as a function of galactic-scale gas properties. [Kruijssen \(2012\)](#) framed this problem in terms of the PDF of the local gas overdensity relative to the mean density in the galactic mid-plane, $x \equiv \rho_g/\rho_0$. For our purposes, it will be convenient to express the PDF in units of stellar density rather than gas density, since the former is the relevant quantity for evaluating the influence of dynamical encounters. We define $y \equiv \rho_*/\rho_0 = x\epsilon(x)$, where ϵ is the local SFE. Then y is the

stellar overdensity with respect to the average gas density ρ_0 . Hence, the stellar density PDF can be written:

$$\frac{\partial p}{\partial y} \propto \frac{\partial p}{\partial x} \left(\epsilon + x \frac{\partial \epsilon}{\partial x} \right)^{-1}. \quad (14)$$

However, we are in fact interested in the fraction of stars per infinitesimal region of overdensity space dy :

$$\frac{\partial \mathcal{F}_*}{\partial y} \propto y \frac{\partial p}{\partial y} \propto \frac{\partial p}{\partial x} \left(x^{-1} + \frac{\partial \ln \epsilon}{\partial x} \right)^{-1}. \quad (15)$$

To evaluate equation 15, the theoretical framework for estimating the gas density distribution and corresponding SFE is briefly reviewed below (for a more complete discussion, see [Kruijssen 2012](#), and references therein).

3.2 ISM properties

3.2.1 Gas density distribution

The PDF of the gas overdensity with respect to the mean gas density in a turbulent region is assumed to be scale-free and follows a lognormal distribution (e.g. [Vazquez-Semadeni 1994](#); [Padoan & Nordlund 2002](#)). It can be written as

$$\frac{\partial p}{\partial x} = \frac{1}{\sqrt{2\pi\sigma_\rho^2 x}} \exp \left\{ -\frac{(\ln x - \overline{\ln x})^2}{2\sigma_\rho^2} \right\}, \quad (16)$$

where the logarithmic mean is

$$\overline{\ln x} = -\sigma_\rho^2/2 \quad (17)$$

and the standard deviation of the density is

$$\sigma_\rho^2 \approx \ln \left(1 + 3b^2 \mathcal{M}^2 \right), \quad (18)$$

where \mathcal{M} is the one-dimensional Mach number, and simulations indicate $b \approx 0.5$ ([Padoan et al. 1997](#); [Federrath et al. 2010](#)).

Throughout this work, we will frequently refer to the properties of gas in the solar neighbourhood and in the CMZ, which we will use as regions for illustrative comparisons. The values \mathcal{M} and ρ_0 in the galactic disc and the CMZ are discussed below in Sections 3.2.2 and 3.2.3.

3.2.2 Connection to galactic properties

We now express the mid-plane density ρ_0 and the Mach number \mathcal{M} in terms of global galactic properties. To estimate these conditions, we follow [Krumholz & McKee \(2005\)](#) in assuming the star-forming galactic disc can be modelled as a gas disc in hydrostatic equilibrium. Then we can write an expression for the [Toomre \(1964\)](#) Q parameter in terms of the mean gas surface density Σ_0 and angular velocity Ω set by the galactic rotation curve:

$$Q \equiv \frac{\kappa \sigma_v}{\pi G \Sigma_0} \approx \frac{\sqrt{2} \Omega \sigma_v}{\pi G \Sigma_0}, \quad (19)$$

where the epicyclic frequency $\kappa = \sqrt{2}\Omega$ for a galaxy with a flat rotation curve, and σ_v is the one-dimensional velocity dispersion. Using equation 19, the mid-plane density for a disc in hydrostatic equilibrium and with scale height h_0 is:

$$\rho_0 = \frac{\Sigma_0}{2h_0} = \frac{\pi G l_p \Sigma_0^2}{2\sigma_v^2} = \frac{l_p \Omega^2}{\pi G Q^2}, \quad (20)$$

where $l_P \approx 3$ is a correction factor for the stellar contribution to the gravitational potential. Considering typical sound speeds in star-forming regions (~ 0.3 km/s), the corresponding Mach number is approximately:

$$M \approx 0.028 l_P^{1/8} Q \left(\frac{\Omega}{1 \text{ Myr}^{-1}} \right)^{-1} \frac{\Sigma_0}{1 M_\odot \text{ pc}^{-2}} \quad (21)$$

where:

$$l_P \approx 10 - 8 f_{\text{GMC}} \quad (22)$$

is the ratio of the mean pressure in a GMC to the mid-plane pressure, and f_{GMC} is the fraction of the ISM mass in GMCs. Empirically, the fraction of molecular gas f_{GMC} is related to the mean surface density (Wong & Blitz 2002; Rosolowsky & Blitz 2005):

$$f_{\text{GMC}} \approx \left[1 + 2.5 \left(\frac{\Sigma_0}{10 M_\odot \text{ pc}^{-2}} \right)^{-2} \right]^{-1}. \quad (23)$$

Finally, a range of values $0.5 < Q < 6$ are observed (Kennicutt 1989; Martin & Kennicutt 2001); we will explore how our results vary with Q .

3.2.3 Properties of the solar neighbourhood and the CMZ

Throughout this work we will use the comparative examples of the solar neighbourhood and the CMZ, with parameters as follows. For the solar neighbourhood, we choose a canonical value of $Q = 1.5$, $\Omega = 2.6 \times 10^{-2}$ Myr and $\Sigma_0 = 12 M_\odot \text{ pc}^{-2}$, in line with Kruijssen (2012). The CMZ occupies the central ~ 250 pc in galactocentric radius of the Milky Way, and exhibits gas properties which vary significantly from those of the disc (e.g. Kruijssen & Longmore 2013; Molinari et al. 2014). The surface density in the CMZ is $\Sigma_0 \sim 1000 M_\odot \text{ pc}^{-2}$ (Guesten & Henkel 1983; Henshaw et al. 2016). We follow Kruijssen et al. (2014) in adopting the same Toomre parameter as in the disc ($Q = 1.5$) for the star-forming circumnuclear stream in the CMZ, at a radius of ~ 100 pc. Kruijssen et al. (2015) find an angular velocity for the stream of $\Omega \approx 1.7 \text{ Myr}^{-1}$.

3.3 Star formation efficiency

3.3.1 Star formation efficiency per free-fall time

Assuming star formation proceeds on a free-fall time τ_{ff} , the SFE ϵ can be expressed in terms of the star formation efficiency per free fall time, ϵ_{ff} . There remains debate on the exact value of ϵ_{ff} (e.g. Elmegreen 2002; Krumholz & Tan 2007; Elmegreen 2007; Padoan & Nordlund 2011; Barnes et al. 2017; Leroy et al. 2017; Hirota et al. 2018; Utomo et al. 2018; Krumholz et al. 2019). While in some regions (often on sub-GMC scales) the value has been found to be up to a factor ~ 5 higher (Evans et al. 2009; Hirota et al. 2018), $\epsilon_{\text{ff}} \approx 0.01$ is found across a wide dynamic range, and we will use this fiducial value in this work.

3.3.2 Star formation time-scale

The integrated SFE at a given density is dependent on the time for which star formation is allowed to proceed, as a

multiple of the free-fall time-scale. The free-fall time-scale at local density ρ_g is

$$\tau_{\text{ff}} = \sqrt{\frac{3\pi}{32G\rho_g}}, \quad (24)$$

and the associated SFE is

$$\epsilon_{\text{fb}} = \frac{\epsilon_{\text{ff}}}{\tau_{\text{fb}}} \tau_{\text{fb}}, \quad (25)$$

where τ_{fb} is the feedback time-scale, the time it takes to halt star formation. The feedback time-scale can be written as the sum of the time until the first supernova ($\tau_{\text{sn}} \sim 3$ Myr) plus the subsequent time until pressure equilibrium between feedback and the surrounding ISM is reached. We refer readers interested in the derivation of τ_{fb} to Kruijssen (2012) and simply quote the result of the calculation here:

$$\tau_{\text{fb}} = \frac{\tau_{\text{sn}}}{2} \left(1 + \sqrt{1 + \frac{2\pi^2 G^2 \tau_{\text{ff}}^2 \Sigma_0^2}{\Phi_{\text{fb}} \epsilon_{\text{ff}}^2 \tau_{\text{sn}}^2 \Omega^2 x}} \right). \quad (26)$$

where Φ_{fb} is a constant which represents the rate at which feedback injects energy into the ISM per unit stellar mass. Its exact value is uncertain (Silk 1997; Mac Low & Ferrara 1999; Efstathiou 2000; Abadi et al. 2003; Dib et al. 2006), and we use an order of magnitude estimate $\Phi_{\text{fb}} \approx 3.2 \times 10^{32} \text{ erg s}^{-1} M_\odot^{-1}$ (see Appendix B in Kruijssen 2012, and references therein).

Fundamentally, this feedback model only includes the energy deposition by supernovae, whereas observations show that ‘early’ feedback mechanisms like photoionisation and stellar winds dominate GMC dispersal (e.g. Kruijssen et al. 2019; Chevance et al. 2019). However, the purpose of our model is not to accurately model the details of the feedback process, but to have a reasonable description of the balance between the energy output of a young stellar population and the kinetic energy density of the ambient interstellar medium. The energy in supernovae is a good proxy for the former (Agertz et al. 2013), and Kruijssen (2012, Appendix C) show that including other feedback mechanisms does not significantly alter the population-integrated SFE when integrating over the complete density PDF.

Where star formation time-scales are long, we wish to limit our consideration to stars which host a disc, i.e. with ages $\lesssim 10$ Myr. In the case where the overdensity $x \rightarrow 0$, we have large $\tau_{\text{fb}} \propto x^{-3/4}$ and $\epsilon_{\text{fb}} \propto x^{-1/4}$. For $\tau_{\text{fb}} > 10$ Myr, we therefore limit our definition of the SFE to those stars formed within $\tau_{\text{inc}} = 10$ Myr of the onset of star formation; at these low overdensities, the ‘incomplete’ SFE is:

$$\epsilon_{\text{inc}} = \frac{\epsilon_{\text{ff}}}{\tau_{\text{ff}}} \tau_{\text{inc}}. \quad (27)$$

In general, we can write the SFE as the minimum of the feedback-limited SFE, the incomplete SFE, and the maximum local SFE. The latter limit is the SFE of protostellar cores ϵ_{core} , obtained by factoring in mass-loss through outflows. We choose $\epsilon_{\text{core}} = 0.5$, consistent with the range $0.25 < \epsilon_{\text{core}} < 0.7$ found by Matzner & McKee (2000). This maximum SFE is attained in the limit of high density. Hence, choosing a different value for ϵ_{core} would just shift the PDF in stellar overdensity above some threshold ($\epsilon_{\text{fb}} > \epsilon_{\text{core}}$) by a factor < 2 (taking $\partial \ln \epsilon / \partial x \rightarrow 0$ in equation 15). We define the SFE as a function of overdensity:

$$\epsilon = \left\{ \epsilon_{\text{fb}}^{-1} + \epsilon_{\text{inc}}^{-1} + \epsilon_{\text{core}}^{-1} \right\}^{-1}. \quad (28)$$

We have chosen this form instead of taking the minimum of the SFEs such that ϵ is differentiable, and therefore equation 15 yields a continuous PDF in density space.

3.4 Hosts of massive stars

In the remainder of this section we convert the stellar density and maximum local star mass distributions into an FUV flux spectrum for fixed local gas overdensity x . When quantifying the FUV flux in star-forming regions, it will be necessary to know whether or not it hosts a massive star. [Fatuzzo & Adams \(2008\)](#) showed that above a certain mass, the contribution of stars to the UV field decreases due to a flattening of the luminosity-mass function (while the IMF remains steep – see also [Armitage 2000](#)). A different realisation of this is apparent in the study of [Winter et al. \(2018b\)](#); they found that for regions of mass $\gtrsim 10^3 M_\odot$, FUV field strength is no longer strongly variable with maximum stellar mass, but is related to the local stellar density. This is a consequence of a well sampled IMF in high stellar mass environments. It is therefore necessary to delineate regions for which stellar density effectively determines FUV flux, from those that are strongly influenced by stochastic variations in the most massive local star.

For the fraction of the stellar population that are born into environments without a well-sampled IMF, calculating the FUV radiation field requires estimating the most massive stellar component, m_{\max} . [Maschberger & Clarke \(2008\)](#) find that the observed distribution of m_{\max} is consistent with random drawing from the IMF. We choose a [Kroupa \(2001\)](#) IMF (equation 6) truncated above $100 M_\odot$ because this is the upper limit of the stellar atmosphere models we adopt in Section 3.5. This is not a problem since the regions with stellar mass $M_c < 10^3 M_\odot$ practically always have $m_{\max} \ll 100 M_\odot$ (and for more massive environments, the maximum FUV luminosity is a weak function of total stellar mass).

3.5 Environment and stellar luminosity

We are now required to define the units of star formation such that we are able to impose some distribution for the luminosity of the most massive *local* star. We wish to evaluate the dependence of the median maximum luminosity $L_{1/2}$ as a function of cluster or association stellar mass M_c . To calculate the FUV luminosity L as a function of star mass m_* we follow the method of [Armitage \(2000](#), see also [Fatuzzo & Adams 2008](#); [Winter et al. 2018b](#)). We use the model grids of luminosities and effective temperatures calculated by [Schaller et al. \(1992\)](#), taking the results for metallicity $Z = 0.02$ (although the luminosity for OB stars does not change significantly in the lower metallicity results) at the output closest to 1 Myr. We then determine the wavelength-dependent luminosity from the atmosphere models by [Castelli & Kurucz \(2004\)](#). To obtain the FUV luminosity, we integrate over the energy range for FUV photons, which is $6 \text{ eV} < h\nu < 13.6 \text{ eV}$. To obtain the median luminosity as a function of total stellar mass in a region, we first draw from the IMF (equation 6) for each M_c to find the median maximum star mass, $m_{1/2}$.

Since we have chosen to assess the FUV luminosity for stars of age 1 Myr, we must consider whether stellar evolution will significantly alter our results. In particular, we are

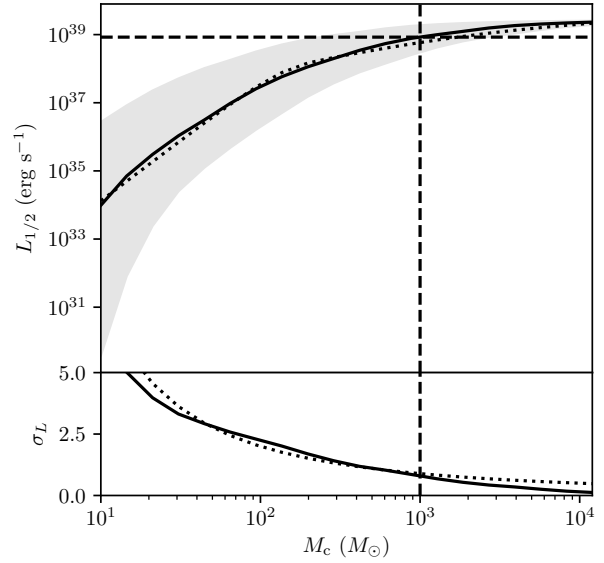


Figure 3. Top: The median luminosity $L_{1/2}$ of the most massive star in a star-forming region with stellar mass M_c with the IMF described by equation 6. The dotted line follows the analytic approximation, equation 29. The vertical dashed line is at the critical mass $M_{\text{crit}} \approx 10^3 M_\odot$ beyond which the local FUV flux is well determined by equation 50. The associated critical luminosity $L_{\text{crit}} \approx 8.4 \times 10^{38} \text{ erg s}^{-1} \text{ cm}^{-2}$ is shown as a horizontal dashed line. The shaded region represents the 1σ deviation in $L_{1/2}$. Bottom: The solid line is the logarithmic standard deviation of the luminosity σ_L , with equation 31 indicated by the dotted line.

interested in whether the FUV flux exposure of PPDs with ages < 10 Myr can be cut short by the death of the most massive stars. We investigate the regions of parameter space for which our static population approximation is appropriate in Appendix A. We find that for the majority of star forming regions, even when the most massive star reaches the end of its lifetime, there is likely to be at least one star with comparable FUV luminosity but main sequence lifetime $\gtrsim 10$ Myr in the region. Thus, the influence of stellar evolution should not significantly effect our statistical conclusions, although may be significant in investigating disc properties in specific regions, especially for individual discs residing in close proximity to the most massive star in the region.

During the course of this work, we will regularly refer to the FUV luminosity of the most massive star in a region, and it will be useful to have an analytic approximation for this parameter. This FUV luminosity for a given total stellar mass M_c is shown in Figure 3. We find that for the critical mass $M_{\text{crit}} = 10^3 M_\odot$, we have $L_{\text{crit}} \approx 8.3 \times 10^{38} \text{ erg s}^{-1}$. The results in Figure 3 again justify our choice for M_{crit} , since above this limit $L_{1/2}$ varies only weakly with M_c . An analytic estimate for the median luminosity follows the form:

$$\Lambda(\phi) \equiv \frac{L_{1/2}(\phi)}{L_{\text{crit}}} \approx \left\{ 1 - e^{-(f_{\text{br}}\phi)^\alpha} \right\} \ln(1 + \phi), \quad (29)$$

where we introduce

$$\phi \equiv \frac{M_c}{M_{\text{crit}}} \quad (30)$$

the ratio of the total stellar mass of the region to the critical mass. Equation 29 has two fitting parameters: $f_{\text{br}} = 8.0$ and $\alpha = 2.55$. The analytic approximation in equation 29 is shown as the dotted line in the top panel of Figure 3. We further define the logarithmic deviation in the maximum luminosity:

$$\sigma_L \approx \frac{8}{(3 + \log \phi)^2}, \quad (31)$$

indicated by the dotted line in the bottom panel of Figure 3 (compared to the direct calculation shown as a solid line). We will further impose the limit $\sigma_L \leq 10$ for numerical reasons, although this is of little practical significance.

We emphasise that equation 29 is simply chosen as a functional form that will permit an intuition for the numerical value of physical variables and simplify our calculations in the following sections. It is appropriate in the range of M_c discussed here under the assumption that the maximum star mass in a region is $\lesssim 100 M_\odot$.

3.6 Initial cluster mass spectrum

In this section we are motivated to find the fraction of stars born in a star-forming region of a given mass. This is obtained via the initial cluster mass function (ICMF), which depends on the galactic environment. We follow [Trujillo-Gomez et al. \(2019\)](#) in assuming that the ICMF follows a modified [Schechter \(1976\)](#) function, additionally truncated from below by a minimum mass:

$$\xi_c \equiv \frac{d\mathcal{F}_c}{dM_c} \propto \phi^{-\beta} \exp\left(-\frac{\phi_{\min}}{\phi}\right) \exp\left(-\frac{\phi}{\phi_{\max}}\right) \quad (32)$$

where $\beta = 2$ is expected due to hierarchical collapse of molecular clouds ([Elmegreen & Falgarone 1996](#)), and $\phi \equiv M_c/10^3 M_\odot = M_c/M_{\text{crit}}$ is proportional to the stellar mass of the star forming region, as usual. Equation 32 is then weighted by ϕ and normalised to give the fraction of stars born in a star-forming region of mass ϕ . In the following we will discuss our choices for ϕ_{\min} and ϕ_{\max} .

3.6.1 Maximum cluster mass

We follow [Reina-Campos & Kruijssen \(2017\)](#) in calculating the maximum stellar mass in a region ϕ_{\max} by considering the most massive molecular cloud that can survive disruption by feedback. The ISM is stable to perturbations with a wavelength longer than the [Toomre \(1964\)](#) length,

$$\lambda_T = \frac{4\pi^2 G \Sigma_0}{\kappa^2} = \frac{2\pi^2 G \Sigma_0}{\Omega^2}, \quad (33)$$

and this is therefore the largest scale on which collapse can take place. The corresponding Toomre mass is:

$$M_T = \frac{\pi \Sigma_0 \lambda_T^2}{4} = \frac{\pi^5 G^2 \Sigma_0^3}{\Omega^4}. \quad (34)$$

Considering the galactic plane as an infinite sheet, the 2D free fall time (collapse within the plane) of a region with radius $\lambda_T/2$ ([Burkert & Hartmann 2004](#)):

$$\tau_{\text{ff},2\text{D}} = \sqrt{\frac{\lambda_T}{2\pi G \Sigma_0}} = \frac{\sqrt{\pi}}{\Omega}. \quad (35)$$

If the feedback time-scale $\tau_{\text{fb}} < \tau_{\text{ff},2\text{D}}$ then the collapsing region will be destroyed by this feedback before the conclusion of collapse, and hence the maximum mass of the GMC is given by:

$$M_{\text{GMC,max}} = f_{\text{coll}} M_T \quad (36)$$

where

$$f_{\text{coll}} = \min\left\{1, \frac{\langle \tau_{\text{fb}} \rangle}{\tau_{\text{ff},2\text{D}}}\right\}^4 \quad (37)$$

is the fraction of mass which survives collapse. We have introduced the feedback time across the entire region, which is:

$$\langle \tau_{\text{fb}} \rangle \approx \tau_{\text{fb}}(x = 1). \quad (38)$$

To convert this into a maximum stellar mass, [Reina-Campos & Kruijssen \(2017\)](#) multiply this by the SFE and the cluster formation efficiency. However, we are not interested here in whether or not a region is bound, and hence we only consider the SFE. We have:

$$\phi_{\max} = \frac{\epsilon_{\text{eff}} f_{\text{coll}} M_T}{M_{\text{crit}}}, \quad (39)$$

where we have defined an effective SFE in the high mass GMC limit. In line with [Reina-Campos & Kruijssen \(2017\)](#), we choose an effective SFE $\epsilon_{\text{eff}} = 0.1$.

3.6.2 Minimum cluster mass

The minimum expected mass for a stellar cluster is more nuanced in this context, and depends on the definition we adopt for a ‘cluster’. As we have already discussed, in the context of this work we are not interested in whether or not a group of stars is initially ‘bound’ in the sense that we aim to find the conditions that a star experiences early in evolution. However, we are interested in the bottom of the hierarchy for early mergers within molecular clouds. We follow [Trujillo-Gomez et al. \(2019\)](#) in deriving this minimum mass by considering a molecular cloud mass dependent SFE:

$$\tilde{\epsilon}_{\text{fb}}(M_{\text{GMC}}) = \frac{\epsilon_{\text{ff}}}{\tau_{\text{ff}}} \tilde{\tau}_{\text{fb}}; \quad \tilde{\epsilon} = \min\{\tilde{\epsilon}_{\text{fb}}, \epsilon_{\text{core}}\}. \quad (40)$$

We find that $\tilde{\epsilon}_{\text{fb}}$ increases with decreasing M_{GMC} for small M_{GMC} , such that below a certain cloud mass:

$$\tilde{\epsilon} \gtrsim \epsilon_{\text{th}} \approx 0.2, \quad (41)$$

where the threshold SFE ϵ_{th} is given by the efficiency required to produce a bound cluster after instantaneous gas expulsion ([Baumgardt & Kroupa 2007](#)). For cloud masses below this limit M_{th} , SFE is high enough to result in hierarchical merging into single objects (which can be considered to be associated within our context), and the minimum mass for a star forming region can be written:

$$\phi_{\min} M_{\text{crit}} = \epsilon_{\text{th}} M_{\text{th}}. \quad (42)$$

We are now left with the problem of solving the equations for the SFE with respect to the galactic scale ISM properties.

In the numerical derivation of ϕ_{\min} we consider the SFE across an entire molecular cloud, $\tilde{\epsilon}$, as opposed to the local SFE considered in Section 3.3, ϵ , which is dependent on x and consistent with the calculation of [Kruijssen \(2012\)](#). The

primary difference is that in the former case, we can estimate the supernova time-scale $\tilde{\tau}_{\text{sn}}$ based on the local stellar mass (but not the influence of density), while in the latter we can assess the influence of local density on the feedback efficiency (but not the variation in supernova time-scale). Ideally we would consider the SFE as a function of both cloud mass and local density. However, this would greatly complicate our prescription, in which we need to define the flux PDF at each stellar density. Instead, we are content to consider $\tilde{\epsilon}$ for the purposes of assessing the minimum stellar mass in a region since these two different prescriptions are physically compatible; $\tilde{\epsilon}$ being SFE on a GMC scale, and ϵ being SFE on a local (stellar) scale.

We refer the reader interested in the derivation of the feedback time-scale to [Trujillo-Gomez et al. \(2019\)](#). In brief, the local gas density used when deriving the SFE as a function of local gas overdensity is replaced by the average cloud density:

$$\rho_{\text{GMC}} = \frac{3}{4} \left(\frac{\pi \Sigma_{\text{GMC}}^3}{M_{\text{GMC}}} \right)^{1/2} = \frac{3}{4} \left(\frac{\pi \Sigma_0^3 f_{\Sigma}^3}{M_{\text{GMC}}} \right)^{1/2}, \quad (43)$$

where we define $f_{\Sigma} \equiv \Sigma_{\text{GMC}}/\Sigma_0$, the ratio between the GMC surface density and the mean gas surface density. Following [Krumholz & McKee \(2005\)](#) and [Kruijssen \(2015\)](#), for a virial ratio $\alpha_{\text{vir}} = 1.3$ (appropriate for pressure confined GMCs – [Bertoldi & McKee 1992](#)) this ratio can be written:

$$f_{\Sigma} = 3.92 \left(\frac{l_P}{2} \right)^{1/2}. \quad (44)$$

In the solar neighbourhood, this yields $\Sigma_{\text{GMC}} \approx 90 M_{\odot} \text{ pc}^{-2}$ (consistent with the findings of [Bolatto et al. 2008](#)). The GMC mass dependent free fall time-scale can be written:

$$\tilde{\tau}_{\text{ff}} = \sqrt{\frac{\pi^{1/2}}{8G}} \left(\frac{M_{\text{GMC}}}{f_{\Sigma}^3 \Sigma_0^3} \right)^{1/4}. \quad (45)$$

Finally, we estimate the time-scale for a supernova to occur by considering the progenitor formation time-scale, which is important at low cloud masses, such that we have:

$$\tilde{\tau}_{\text{sn}} = \tau_{\text{sn}} + \Delta\tau_{\text{sn}}, \quad (46)$$

where we have defined $\Delta\tau_{\text{sn}}$ as the time it takes for the stellar component of a star-forming region to reach a sufficient mass to form an OB star. This mass is calculated by [Trujillo-Gomez et al. \(2019\)](#) to be $M_{\text{OB}} \approx 99 M_{\odot}$, and the corresponding time-scale:

$$\Delta\tau_{\text{sn}} = \frac{M_{\text{OB}} \tilde{\tau}_{\text{ff}}}{M_{\text{GMC}} \epsilon_{\text{ff}}}. \quad (47)$$

With these adjustments, an alternate version of equation 26 is:

$$\tilde{\tau}_{\text{fb}} \approx \frac{\tilde{\tau}_{\text{sn}}}{2} \left[1 + \sqrt{1 + \frac{2\sqrt{2G}\pi^{3/4}l_P\Sigma_0^2 M_{\text{GMC}}^{3/4}}{3\Phi_{\text{fb}}\epsilon_{\text{ff}}\tilde{\tau}_{\text{sn}}^2\Sigma_{\text{GMC}}^{9/4}}} \right]. \quad (48)$$

We can solve the system of equations 40 to 48 for M_{th} such that

$$\tilde{\epsilon}|^{M_{\text{th}}} = \epsilon_{\text{th}}, \quad (49)$$

to find ϕ_{min} (i.e. the minimum mass of a star forming region). From the above formulation there is no physical reason why we cannot have $\phi_{\text{min}} > \phi_{\text{max}}$. In this case, the bottom of the hierarchy exceeds the maximum mass that can be

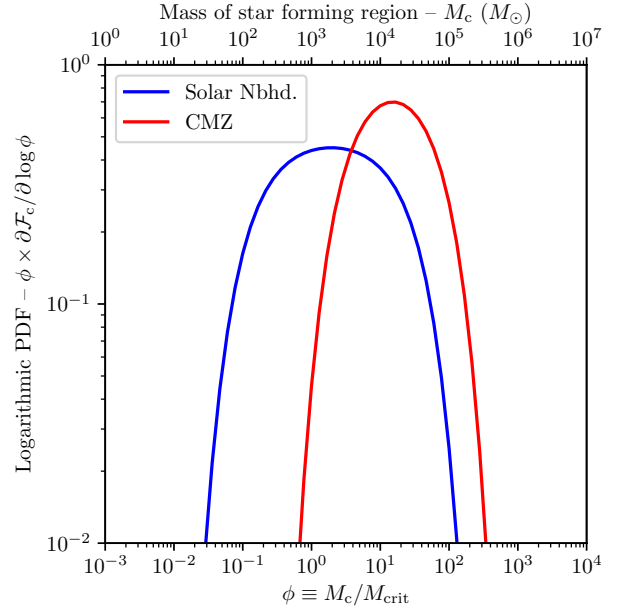


Figure 4. The ICMF in terms of $\phi \equiv M_c/M_{\text{crit}}$ weighted by the stellar mass of the region, indicating the fraction of stars born in such an environment. The lower limit ϕ_{min} is given by the bottom of the single-object merger hierarchy calculated by [Trujillo-Gomez et al. \(2019\)](#). The maximum stellar mass of a region ϕ_{max} is the stellar component of a GMC with mass given by the feedback-limited fraction of the Toomre mass ([Reina-Campos & Kruijssen 2017](#)). The blue line is for the solar neighbourhood, while the red line describes the ICMF in the CMZ.

produced in such an environment, and the former is therefore set by the latter. This results in a narrow distribution of stellar masses, and $\phi_{\text{min}} = \phi_{\text{max}}$ (set by the maximum possible mass), such that our ICMF continues to be physically valid. For numerical reasons, it will also be convenient to set limits on the allowed values for ϕ_{min} and ϕ_{max} . We define $\phi_{\text{max,min}} = \phi_{\text{min,min}} = 10^{-2}$, $\phi_{\text{min,max}} = 100$ and $\phi_{\text{max,max}} = 10^6$. Our results are not strongly sensitive to these choices since the FUV flux experienced by PPDs is insensitive to the stellar mass of the star-forming region in the high and low mass limits (see Section 3.7).

3.6.3 Derived initial cluster mass function

The theoretical ICMFs of the solar neighbourhood and CMZ are shown in Figure 4, weighted by mass to illustrate the fraction of stars initially found in a region of a given mass. We note that our upper mass estimates are somewhat larger than those of [Reina-Campos & Kruijssen \(2017\)](#) since we are not interested in the cluster formation efficiency. We find that regions in the CMZ have $\phi_{\text{min}} = 3.1$ (i.e. minimum mass $M_{\text{min}} = 3.1 \times 10^3 M_{\odot}$) and $\phi_{\text{max}} = 74$ (i.e. maximum mass $M_{\text{max}} = 7.4 \times 10^4 M_{\odot}$), while the solar neighbourhood has $\phi_{\text{min}} = 0.13$ (i.e. $M_{\text{min}} = 130 M_{\odot}$) and $\phi_{\text{max}} = 33$ (i.e. $M_{\text{max}} = 3.3 \times 10^4 M_{\odot}$). These adopted minimum masses are the same as those quoted in [Trujillo-Gomez et al. \(2019\)](#). While we do not compare the ICMF here to the observed distribution of young star forming regions, this exercise is performed in the latter study, wherein the theoretical ICMF is found to be in good agreement with the existing observational constraints.

3.7 FUV flux distribution

To build a distribution of FUV flux as a function of local density, we are motivated to quantify the expected (mean) flux F_0 . We now outline a model motivated by theory and observations to find $F_0(x, \phi)$ for fixed ISM properties.

3.7.1 High mass clustered environment regime

For high mass star-forming regions, the FUV flux is closely related to the stellar density ρ_* (Winter et al. 2018b). Empirically, the mean FUV flux in high mass environments is

$$F_0^{\text{HM}} \approx 1000 \left(\frac{\rho_*}{1 M_\odot \text{pc}^{-3}} \right)^{1/2} G_0. \quad (50)$$

We will assume that for small ϕ , as the mass of the local environment increases the flux distribution approaches this average. This is an empirical relationship. Since the stars which dominate the local FUV flux (of mass $\sim 30\text{--}50 M_\odot$ – e.g. Armitage 2000) make up only a small fraction of the IMF ($\sim 10^{-3}$), equation 50 is determined by the radial stellar density profile of star-forming regions rather than the local density of OB stars.

3.7.2 Flux in the field

To define the full PDF of FUV flux for a given density, it will be further necessary to define a minimum value for which the FUV exposure is set by the field strength between star-forming regions, dependent on their separation λ_0 . For an ISM which is shaped by expanding bubbles driven by stellar feedback, the separation is set by the scale on which the bubbles depressurise, which is the scale height of the disc (McKee & Ostriker 1977; Hopkins et al. 2012). Kruijsen et al. (2019) recently confirmed this empirically for the nearby spiral galaxy NGC300 across all galactocentric radii in the range 0–3 kpc (or out to $\sim 0.5R_{25}$). We must also consider the limit where the mean GMC radius:

$$\langle R_{\text{GMC}} \rangle = \int d\phi \xi_c \sqrt{\frac{M_{\text{GMC}}(\phi)}{\pi \Sigma_0 f_\Sigma}} \quad (51)$$

becomes greater than h_0 (regions of large Ω). In this case, $M_{\text{GMC}}(\phi)$ can be found by solving:

$$\tilde{\epsilon}(M_{\text{GMC}}) M_{\text{GMC}} = M_{\text{crit}} \phi \quad (52)$$

to give $\langle R_{\text{GMC}} \rangle$. Then we have:

$$\lambda_0 = 2 \cdot \max \{ h_0, \langle R_{\text{GMC}} \rangle \}. \quad (53)$$

We must also consider the extinction of FUV photons due to the surface density of gas between star-forming regions:

$$\Sigma_{\text{eff}}^f = 2\rho_0 \lambda_0 x = \frac{\Sigma_0 \lambda_0}{h_0} x, \quad (54)$$

where ρ_0 is related to Σ_0 and h_0 by equation 20. We define an extinction factor:

$$C_{\text{ext}} \equiv \frac{\Sigma_0}{13.36 M_\odot \text{pc}^{-2}}, \quad (55)$$

where we have normalised the mean surface density by the column density required for 1 mag of extinction in the FUV.

This normalisation is calculated from the ratio of extinction in FUV to the visible $A_{\text{FUV}}/A_V \approx 2.7$ (Cardelli et al. 1989) and the column density of hydrogen required for 1 mag of extinction in the visible $N_{\text{H}}/A_V = 1.8 \times 10^{21} \text{ cm}^{-2} \text{ mag}^{-1}$ (Predehl & Schmitt 1995).

Finally, we must also consider star-forming regions occupied by many OB stars, which matters when the fractional variation of distances between sources becomes small (i.e. for a star well outside of a star-forming region). This can be accounted for weighting flux contributions by stellar mass for regions with more than one strong FUV source:

$$\phi_{>1} = \max\{1, \phi\}. \quad (56)$$

This consideration highlights the importance of our normalisation for ϕ , chosen such that the FUV luminosity of the most massive star is only logarithmically dependent on ϕ for $\phi > 1$ (equation 29). The factor $\phi_{>1}$ addresses the weighted contribution of the the most massive star-forming regions to the average FUV field in a given galactic environment.

With the above considerations, the FUV field strength between star-forming regions can now be calculated by the weighted contribution from the star-forming regions multiplied by an extinction factor:

$$F_0^f = \frac{L_{\text{crit}}}{\lambda_0^2} \int d\phi \phi_{>1} \xi_c(\phi) \Lambda(\phi) \cdot \int dx \exp\left(-\frac{C_{\text{ext}} \lambda_0}{h_0} x\right) \frac{\partial p}{\partial x}. \quad (57)$$

In the Solar neighbourhood this calculation yields $F_0^f = 0.8 G_0$ (close to the empirical estimate by Habing 1968) and for the CMZ we obtain $F_0^f = 2200 G_0$.

3.7.3 Low mass clustered environments

Low mass environments do not have a well sampled IMF, but may still represent regions of high density. For such a region the flux is dependent on the most massive stellar component. In a statistical sense, this is in turn dependent on the mass of the star-forming region. We require a functional form for which the average FUV flux F_0 at a given stellar density is proportional to the average luminosity of the most massive neighbour Λ , but is limited in the low mass limit by F_0^f :

$$\psi_0 = \Lambda + \psi_0^f. \quad (58)$$

We have defined the ratio of the average local flux to the high mass limit $\psi_0 \equiv F_0/F_0^{\text{HM}}$, with $\psi_0^f = F_0^f/F_0^{\text{HM}}$. The normalisation scale $F_0^{\text{HM}}(\rho_*)$ is a function of density, and since $F_0^{\text{HM}} \rightarrow 0$ as $\rho_* \rightarrow 0$ we have $\psi_0^f \gg 1$. In this limit it follows that $\psi_0 \approx \psi_0^f$, and the PDF for ψ_0 is:

$$\left. \frac{\partial \mathcal{F}_*}{\partial \psi_0} \right|_{\rho_* \rightarrow 0} \rightarrow \delta(\psi_0 - \psi_0^f) \quad (59)$$

where δ is a Dirac delta function (for fixed ρ_* or, equivalently, x). In the lower limit ($\psi_0 < \psi_0^f$), no corresponding Λ exists and we have:

$$\left. \frac{\partial \mathcal{F}_*}{\partial \psi_0} \right|_{\psi_0 < \psi_0^f} = 0, \quad (60)$$

for all x . Above this threshold, we can evaluate Λ for a given value ψ_0 and write the PDF:

$$\left. \frac{\partial \mathcal{F}_*}{\partial \psi_0} \right|_{\psi_0 > \psi_0^f} = \frac{\partial \mathcal{F}_*}{\partial \phi} \left| \frac{\partial \phi}{\partial \psi_0} \right| = \frac{\partial \mathcal{F}_*}{\partial \phi} \left| \frac{\partial \Lambda}{\partial \phi} \frac{\partial \phi}{\partial \Lambda} \right| = \frac{\partial \mathcal{F}_*}{\partial \phi} \left| \frac{\partial \Lambda}{\partial \phi} \right|^{-1}, \quad (61)$$

where $\partial\Lambda/\partial\phi$ can be obtained from equation 29.

To evaluate the PDF with respect to ϕ , we consider the (normalised) ICMF defined in Section 3.6:

$$\frac{\partial\mathcal{F}_*}{\partial\phi} \propto \phi\xi_c(\phi). \quad (62)$$

We have multiplied the ICMF by a factor ϕ since the number of stars within a star-forming region scales with stellar mass. Hence the PDF for FUV flux, equation 61, can be expressed analytically at a fixed overdensity x .

We are additionally interested in the influence of extinction of FUV photons due to the molecular gas present in the nascent cluster or association. The calculation of an equivalent extinguished normalised mean flux ψ_0^{ext} requires further assumptions regarding the initial distribution of stars and gas. These are reviewed in Appendix B where we calculate the quantities relevant in producing an upper limit on the influence of extinction.

3.7.4 Dispersion from mean FUV flux

Equation 61 defines a PDF for the mean flux distribution for fixed density, but in deriving it we have assumed that all star-forming regions of a fixed mass exhibit the same flux distribution. This is clearly not the case, as the most massive star and the internal density profile can yield variations in the flux experienced by the stellar population. To model these variations, we consider deviations from the average flux ratio ψ_0 which follow a lognormal distribution:

$$\frac{\partial\mathcal{F}_*}{\partial\delta\psi} = \frac{1}{\sqrt{2\pi\sigma_F^2\delta\psi}} \exp\left\{-\frac{(\ln\delta\psi)^2}{2\sigma_F^2}\right\} \quad (63)$$

where $\delta\psi \equiv \psi/\psi_0$ and $\psi = F/F_0^{\text{HM}}$. The logarithmic flux dispersion σ_F is the contribution of the dispersion σ_F^f in flux arising from varying spatial separations from ionising sources, and the dispersion σ_L in the luminosity of the most massive member of the region. The former dominates the dispersion in the limit where FUV flux is determined by the field value, and in the limit of massive environments where σ_L is small. In the intermediate regime, the dispersion is dominated by σ_L . Hence we have:

$$\sigma_F = \sigma_F^f + \sigma_L(\phi) \cdot \mathcal{W}(\psi_0) \quad (64)$$

where we estimate $\sigma_F^f = 0.5$ (approximated from the results of Winter et al. 2018b). The weighting function is defined:

$$\mathcal{W} = \max\left\{\text{erf}\left(\frac{\ln\psi_0 - \ln\psi_0^f}{\sqrt{2}\sigma_F^f}\right), 0\right\}. \quad (65)$$

We have used σ_F^f as the deviation in the (logarithmic) error function such that $\sigma_F \rightarrow \sigma_F^f$ in this range around ψ_0^f . Otherwise the contribution from σ_L could result in a significant fraction of stars falling below the field flux threshold.

Since ψ is the product of ψ_0 and $\delta\psi$, we can evaluate its PDF using equations 61 and 63:

$$\frac{\partial\mathcal{F}_*}{\partial\psi} = \int d\psi_0 \frac{\partial\mathcal{F}_*}{\partial\psi_0} \frac{\partial\mathcal{F}_*}{\partial\delta\psi} \frac{1}{\psi_0}. \quad (66)$$

Hence, we have a PDF for the FUV flux experienced by a stellar population at a fixed overdensity x .

To calculate the extinguished flux, the above prescription

cannot be applied, because we already needed to marginalise over ϕ in the initial calculation of the PDF for ψ_0^{ext} (see Appendix B). To simplify, we assume $\sigma_F = \sigma_F^f$ as a first order estimate. While this underestimates the dispersion in flux for intermediate ϕ values, we perform these calculations to give a sense of the severity of FUV extinction for the most extreme regions. In this case, the flux dispersion is $\sigma_F \sim \sigma_F^f$ anyway. As discussed in Appendix B, more detailed estimates of the true influence of extinction are required, and we leave this for future work.

3.8 Stellar density–FUV flux distribution

3.8.1 No extinction

To illustrate the consequences of the formulation we have presented in this section, we now apply our results to the solar neighbourhood and the CMZ with parameters indicated in Sections 3.2.3. The PDF for stars in terms of the local stellar density and FUV flux is given by:

$$\frac{\partial^2\mathcal{F}_*}{\partial\rho_*\partial F} = \frac{\partial\mathcal{F}_*}{\partial\rho_*} \frac{\partial\mathcal{F}_*}{\partial F} \propto \frac{\partial\mathcal{F}_*}{\partial y} \frac{\partial\mathcal{F}_*}{\partial\psi}, \quad (67)$$

where the last expression is evaluated using equations 15 and 66. The results of this calculation are shown in Figure 5 in the case of no interstellar extinction. We have indicated contours of equal dispersal time-scale for $\tau_{\text{disp}} = 1, 2$ and 3 Myr for a star of mass $0.5M_\odot$ hosting a PPD with $\alpha = 5.4 \times 10^{-3}$ (as calculated in Section 2).

Although the sample of young star-forming regions compiled by Winter et al. (2018b) is not complete, we can qualitatively compare our results in Figure 5, where we overplot contours for some observed star-forming environments. In agreement with Winter et al. (2018b), we find that stars do not occupy regions of high density and low FUV flux such that disc dispersal would be driven by dynamical encounters (i.e. external photoevaporation dominates). In the solar neighbourhood the most extreme F and ρ_* lies at $F \sim 10^5 G_0$ and $\rho_* \sim 10^4 M_\odot \text{pc}^{-3}$. This is equivalent to the conditions within the core of the Orion Nebula Cluster (ONC); the most extreme observed environment in the solar neighbourhood in terms of these parameters (see Winter et al. 2019a, for a discussion of photoevaporated PPDs in such an environment). The lower limit in FUV flux is $\sim 1 G_0$, which is the observed field value in the solar neighbourhood (Habing 1968). Additionally, we predict a number of regions with low $F \sim 1\text{--}10 G_0$, but $\rho_* \sim 10^3 M_\odot \text{pc}^{-3}$. This reflects the conditions observed in Lupus for example (Nakajima et al. 2000; Merín et al. 2008; Cleeves et al. 2016; Haworth et al. 2017). In summary, the distribution of stellar environments is in good agreement with what we would expect from observations of local regions.

In the case of the CMZ, we find much higher typical FUV field strengths and densities. The most extreme regions lie at $\rho_* \sim 10^6 M_\odot \text{pc}^{-3}$ and $F \sim 10^6 G_0$. This is comparable to the conditions found in core of Arches and Westerlund 1 (Figer et al. 1999; Mengel & Tacconi-Garman 2007; Winter et al. 2018b). The contour for Quintuplet is lower density and experiences lower FUV flux than the majority of stars as predicted by our model. This may be due to dynamical evolution of the cluster, which is older and lower mass than Arches. The velocity dispersion in Arches is $\sim 5.4 \text{ km/s}$

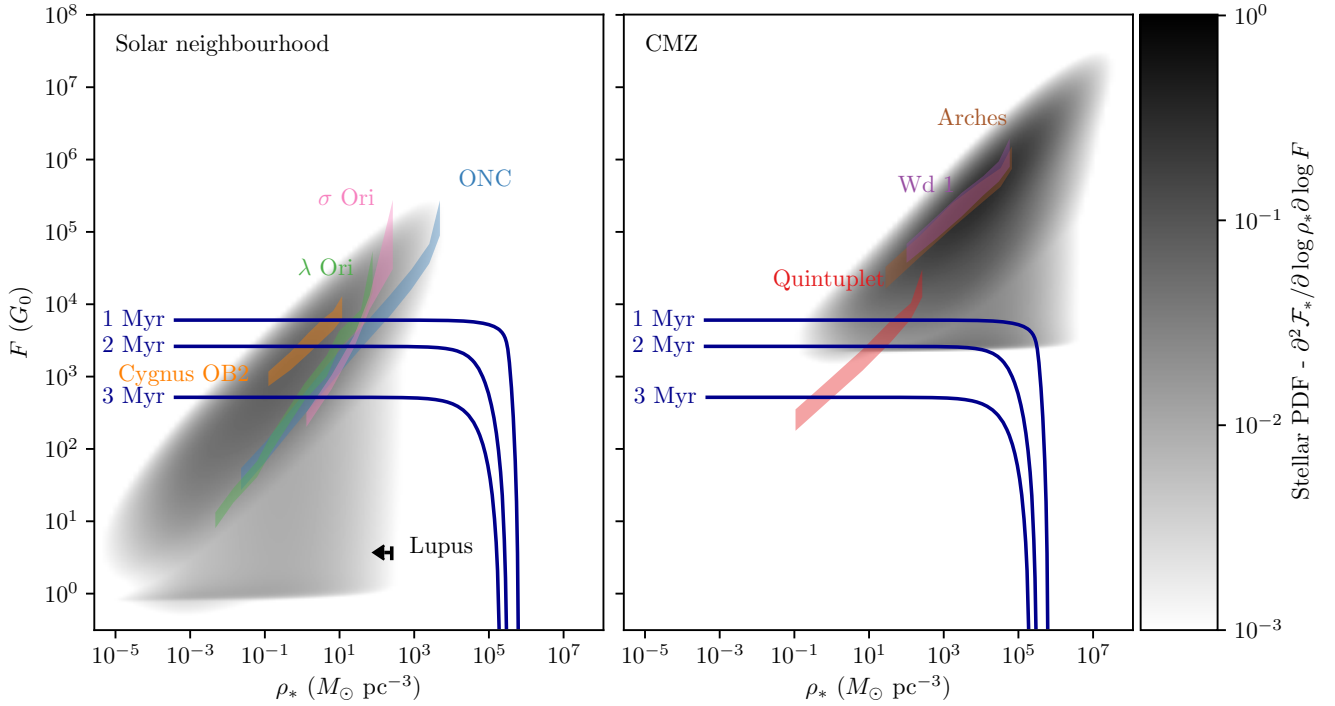


Figure 5. Two dimensional PDF for stars in F - ρ_* (FUV flux–stellar density) space. The left panel is for the solar neighbourhood, described by mean surface density $\Sigma_0 = 12 M_\odot \text{ pc}^{-2}$, Toomre $Q = 1.5$, and angular speed $\Omega = 2.6 \times 10^{-2} \text{ Myr}^{-1}$. The right panel reflects conditions in the CMZ, with $\Sigma_0 = 1000 M_\odot \text{ pc}^{-2}$, $Q = 1.5$ and $\Omega = 1.7 \text{ Myr}^{-1}$. We have marked contours in the PPD dispersal time-scale calculated with the model described in Section 2 for a star of mass $m_* = 0.5 M_\odot$ (approximately the mean mass stellar mass from our IMF) with a viscosity parameter $\alpha = 5.4 \times 10^{-3}$. We have additionally indicated some empirically derived contours calculated by Winter et al. (2018b) for a number of young stellar environments, truncated at a radius such that 90% of stars for each region are included.

(Clarkson et al. 2012), while Quintuplet may have a velocity dispersion as high as 10 km/s (Stolte et al. 2014). Given Quintuplet’s present day stellar density, this upper limit is consistent with a supervirial dynamical state, such that it is possible that it has undergone an epoch of expansion. In addition, the contours presented in Winter et al. (2018b) used a conservative estimate for the maximum stellar mass, and did not account for the contribution of the field flux at large radii. In general, the distribution of stellar birth environments in the CMZ suggest that both FUV photons and dynamical encounters play a role in PPD evolution (although for the majority of discs, external photoevaporation remains the dominant dispersal mechanism), and that discs cannot survive for long in such environments.

3.8.2 Maximal Extinction

In Appendix B, we estimate the effect of extinction on the FUV flux distribution by assuming Plummer sphere geometry of the gas within a star-forming region. We then integrate over a radial coordinate defined to be consistent with the total stellar mass to calculate the resulting surface density if the most massive star is at the centre of the region. The gas surface density is then used to calculate the reduction in FUV flux a star experiences.

The result of incorporating interstellar extinction into our calculations is shown in Figure 6. Our results indicate very high degrees of extinction at high local gas densities

ρ_g , and hence we find that many regions where PPDs that would otherwise be dispersed quickly by FUV photons are efficiently shielded during the embedded phase. Apart from the contours for τ_{disp} due to dynamical encounters and external photoevaporation, we have further indicated a canonical limit above which gas density rapidly alters disc evolution through ram pressure. In the case of the CMZ, the majority of stars that experience large FUV extinction fall into this region, and hence we would expect the ISM to play an important role in PPD evolution prior to gas expulsion.

As we discuss in Appendix B, the prescription we have implemented for FUV extinction is expected to underestimate the apparent FUV flux experienced by a given star since we have assumed that the local gas density distribution follows a Plummer density profile. This is not the case for a realistic, clumpy gas distributions, which reduce the efficiency of extinction. Hence, the results of our calculations summarised in this section do not offer conclusive answers to the nature of disc evolution during the embedded phase, but rather highlight the importance of the following issues for disc evolution:

- (i) The time-scale of the embedded phase (e.g. Kruijssen et al. 2019).
- (ii) The efficiency of extinction during the embedded phase (e.g. Ali & Harries 2019).
- (iii) The (statistical) influence of ram pressure stripping

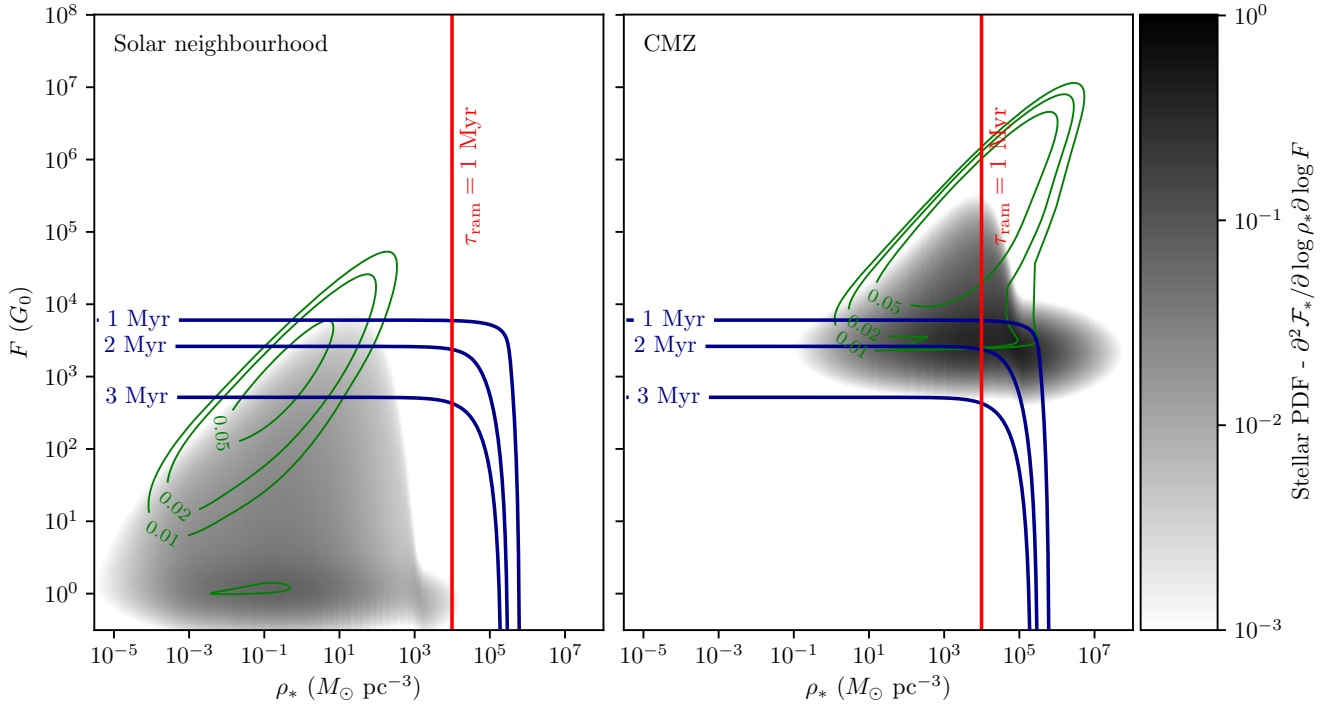


Figure 6. As in Figure 5, but including a prescription for the maximal FUV extinction by the ambient gas. The vertical red line marks the stellar density threshold above which ram pressure due to the ambient gas will alter disc evolution on time-scales $\lesssim 1$ Myr for a star with $m_* = 0.5 M_\odot$ (see the text for details). The green contours are the PDF values without extinction (Figure 5) for comparison. We do not indicate the empirical contours in this case, because Winter et al. (2018b) did not account for extinction in their calculation of the FUV flux.

on a PPD population as a function of local gas density (e.g. Bate 2018; Kuffmeier et al. 2018).

In order to fully understand how PPD properties evolve, these three questions must be addressed. Despite these uncertainties, in the case of the CMZ even our calculation for the flux between star-forming regions is sufficient to significantly reduce PPD lifetimes $\tau_{\text{disp}} \lesssim 3$ Myr. However, we have assumed this lower limit in flux is unaffected by local FUV extinction. We justify this assertion by arguing that, since the field flux F^f is the sum of contributions from all directions, the clumpiness of the gas distribution makes it likely that it is only reduced by a factor of order unity when averaged over time (dependent on the solid angle subtended by the gas). This assertion requires validation in terms of a realistic treatment of extinction (point ii). For the remainder of this work, we will focus on the lifetimes of discs post-gas expulsion.

4 DISCUSSION

4.1 Dispersal time-scale distribution

When answering the question of planet formation efficiency within a given environment, it is of major importance to understand the expected distribution of PPD lifetimes. In environments where a large fraction of stars have discs that are quickly dispersed by stellar feedback, we might expect a low planet formation efficiency. For this purpose, we can

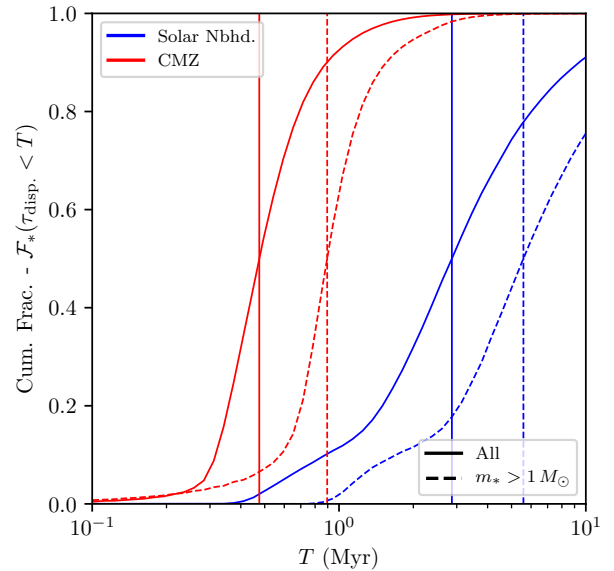


Figure 7. Cumulative fraction of discs with $\tau_{\text{disp}} < T$ in the solar neighbourhood (blue lines) and CMZ (red lines), as set by external disc dispersal mechanisms. We show the distributions for all discs (solid lines) and discs for which the host star has a mass $> 1 M_\odot$ (dashed lines). The vertical lines of corresponding colour and style mark the median disc lifetimes for each PPD sample. We have again assumed a viscosity parameter $\alpha = 5.4 \times 10^{-3}$.

write the fraction of PPDs with a given lifetime τ_{disp} for fixed τ_{visc} :

$$\frac{\partial \mathcal{F}_*}{\partial \tau_{\text{disp}}} = \int dF \int dm_* \frac{\partial \mathcal{F}_*}{\partial F} \frac{\partial \mathcal{F}_*}{\partial m_*} \frac{\partial \mathcal{F}_*}{\partial \rho_*} \left| \frac{\partial \tau_{\text{disp}}}{\partial \rho_*} \right|^{-1} \quad (68)$$

where $\partial \mathcal{F}_* / \partial m_* = \xi_*$ is the stellar IMF (we can integrate over flux or stellar density interchangeably here).

The results of this calculation are presented as a cumulative distribution of τ_{disp} for the stellar population in Figure 7. We find that if we consider PPDs around all stars down to $0.08 M_\odot$ with our chosen IMF, then we obtain median dispersal time-scales of 2.9 Myr in the solar neighbourhood and 0.5 Myr in the CMZ. In both cases these medians are below the characteristic PPD lifetimes for non-photoevaporated populations ($\sim 3\text{--}10$ Myr). However, if we instead consider only PPDs with host stars above $1 M_\odot$, then the median dispersal time-scales increase to 5.6 Myr in the solar neighbourhood, and 0.9 Myr in the CMZ. This highlights the large difference between the expected lifetimes of discs around low- and high-mass stars under the influence of external photoevaporation. For all stellar masses, disc lifetimes are suppressed by a factor $\gtrsim 5$ in the CMZ with respect to the solar neighbourhood. This finding has significant consequences for PPD evolution in the central ~ 250 pc of the Milky Way, where the time and material available for planet formation is severely reduced by dispersal mechanisms (primarily external photoevaporation). Indeed, for the whole stellar population, $\sim 90\%$ of PPDs are dispersed within 1 Myr of the destruction of the parent GMC due to external dispersal mechanisms alone.

4.2 Gas properties & PPD dispersal

To explore the parameter space for ISM properties and host stellar mass, we rewrite equation 68 in terms of a fixed stellar mass:

$$\frac{1}{2} = \int_0^{\tau_{\text{disp},1/2}} d\tau_{\text{disp}} \int dF \frac{\partial \mathcal{F}_*}{\partial F} \frac{\partial \mathcal{F}_*}{\partial \rho_*} \left| \frac{\partial \tau_{\text{disp}}}{\partial \rho_*} \right|^{-1} \quad (69)$$

to solve numerically for the median dispersal time-scale $\tau_{\text{disp},1/2}$. In Figure 8 we show $\tau_{\text{disp},1/2}$ as a function of gas surface density Σ_0 , and angular velocity Ω within a galactic disc for varying Toomre Q , and stellar host mass m_* . Most obviously, the time-scale for PPD destruction generally decreases with increasing Σ_0 . This relationship is simply due to increasing stellar density and maximum mass for a star-forming region with increasing Σ_0 , leading to greater FUV flux. The opposite is true for Q , and therefore τ_{disp} increases with increasing Q . The increase in τ_{disp} with increasing host mass is due to the greater efficiency of external photoevaporation acting on discs around lower mass stellar hosts, since they have a reduced gravitational potential and therefore smaller gravitational radius within the disc (see Haworth et al. 2018a,b; Winter et al. 2019b).

The dependence of τ_{disp} on Ω is more complicated, and competing factors dictate the relationship. Firstly, larger Ω means larger ρ_0 (equation 20), and hence higher densities. However, this also means larger field flux is reduced by greater gas surface density (and therefore extinction). A high angular velocity also restricts the maximum cluster or association mass (equation 34) and therefore reduces the local maximum FUV luminosity, unless Ω is sufficiently small

such that $\langle \tau_{\text{fb}} \rangle < \tau_{\text{ff},2D}$ (equations 35 and 37). In general, high angular velocities decrease the efficiency of externally induced disc dispersal.

Finally, we find that the position of the solar neighbourhood in the parameter space (marked by a blue dot in the middle panel of Figure 8) is approximately at the maximum surface density where the majority of the disc population around stars with $m_* \sim 1 M_\odot$ do not get significantly depleted by external influences ($\tau_{\text{disp}} \approx 4$ Myr). This is intriguing because it suggests that the position of the solar system within the galaxy is such that a maximal *number* (not fraction) of stars have PPDs which disperse largely by internal processes (including planet formation). Since the time and material available for planet formation must influence the planets that are capable of forming, we tentatively suggest that the solar neighbourhood is therefore a special region in terms of galactic environments and exoplanet properties (and possibly frequency). Future studies may contextualize this hypothesis in terms of theoretical and observed galactic-scale ISM properties to establish the degree to which the solar neighbourhood is a special case for planet formation.

5 CONCLUSIONS

We have presented the first comprehensive theoretical prescription for linking star formation parameters to PPD dispersal time-scales due to FUV-induced photoevaporation, dynamical encounters and ram pressure stripping. This has numerous applications for assessing the planet formation potential of star-forming regions, and establishing the typical influences on PPD evolution for future investigation. We summarise our main findings as follows:

- (i) The solar neighbourhood lies close to the largest ISM surface density for which the majority of the PPD population are not influenced by external dispersal mechanisms. At larger surface densities, PPDs have lifetimes that are significantly shortened by (predominantly) FUV flux.
- (ii) Due to the higher gas densities in the CMZ, much of the stellar population initially experiences high FUV flux. This results in dispersal time-scales that are a factor $\gtrsim 5$ shorter than those in the solar neighbourhood. Across the entire stellar mass range, we predict that $\sim 90\%$ of PPDs are destroyed within 1 Myr in the CMZ. Therefore, we expect that planet formation in this region is severely limited in terms of available time and mass.
- (iii) As found by Winter et al. (2018b), external photoevaporation is the dominant mechanism for disc dispersal in the solar neighbourhood, and we find that no stars exist in regions where dynamical encounters can truncate PPDs. Extending this to the CMZ, we find that the time-scale for FUV-induced disc destruction remains shorter than the time-scale for tidal disruption.
- (iv) We estimate an upper limit on the influence of extinction on the FUV flux. Our calculations suggest that PPDs in high density regions ($\rho_* \gtrsim 10^3 M_\odot \text{ pc}^{-3}$ in the solar neighbourhood, $\rho_* \gtrsim 10^4 M_\odot \text{ pc}^{-3}$ in the CMZ) can be efficiently shielded by ambient gas. In this case dynamical encounters remain insignificant as a depletion mechanism since the ram pressure imposed on a disc population operates on a much shorter time-scale $\tau_{\text{ram}} \ll \tau_{\text{tidal}}$ (in agreement with Wijnen

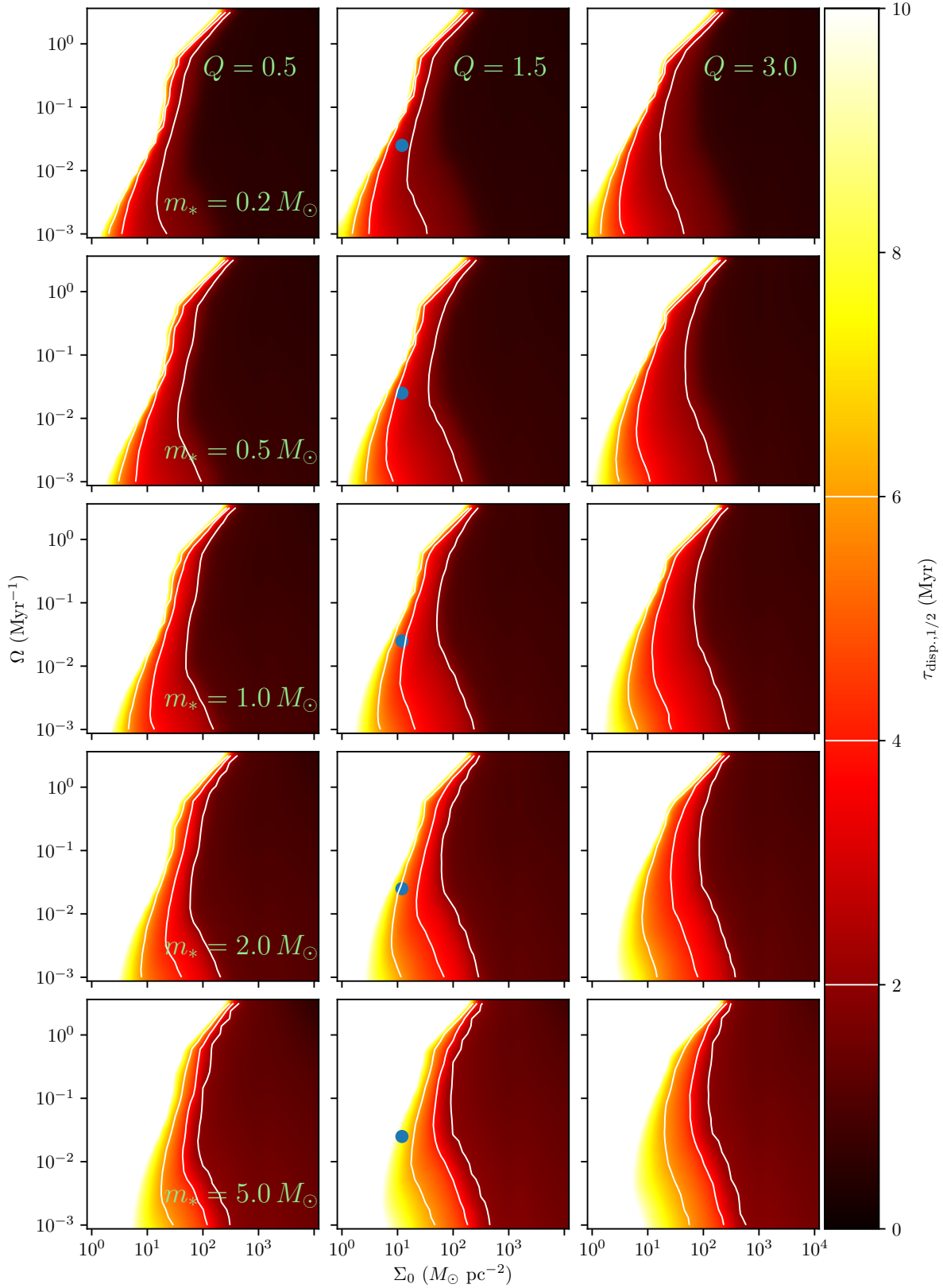


Figure 8. The median dispersal time-scales $\tau_{\text{disp},1/2}$ induced by external photoevaporation and dynamical encounters for PPDs around a star of mass $m_*/M_\odot = \{0.2, 0.5, 1.0, 2.0, 5.0\}$ (from top to bottom) as a function of gas surface density Σ_0 and angular velocity Ω , for Toomre $Q = \{0.5, 1, 3\}$ (from left to right). The blue circle marks the position of the solar neighbourhood and corresponds to the Sun in the middle panel ($m_* = 1 M_\odot$). Regions of parameter space for which $\tau_{\text{disp},1/2} < 10$ Myr exhibit disc lifetimes that are significantly reduced with respect to a PPD evolving in isolation. White contours are placed at 2, 4 and 6 Myr.

et al. 2017b). We therefore conclusively rule out dynamical encounters as the dominant dispersal mechanism in any environment. However, incidental PPD destruction by dynamics remains possible due to the intrinsic stochasticity of this mechanism. For CMZ-like regions, the ram pressure influences PPDs on a short time-scale in all regions where FUV flux is severely reduced by extinction.

In addition to providing insights into the link between star formation physics and planet formation, our findings also highlight particular questions for future work to answer. For each of the above findings we summarise some such issues:

(i) Is the solar neighbourhood special? Future studies may combine calculations for the number of stars born in a given environment with the expected disc dispersal time-scales we have calculated here. In this way, statistical conclusions can be drawn regarding the significance of the position of the solar neighbourhood in Σ_0 - Ω space.

(ii) What is the observed fraction of stars that have discs in the CMZ as a function of age? Early investigations on this topic suggest low disc fractions of a few percent in the Arches cluster (Stolte et al. 2010, 2015).

(iii) How long is the typical viscous time-scale for PPDs? We have assumed a viscous time-scale of $\tau_{\text{visc}} = 1$ Myr for a star of mass $1 M_{\odot}$ (broadly consistent with measured accretion rates – e.g. Manara et al. 2016). We find that the dispersal time-scale, when dominated by photoevaporation, scales as $\tau_{\text{disp}} \approx \tau_{\text{FUV}} \propto \tau_{\text{visc}}^{0.7}$, and hence our findings are moderately dependent on the true value of τ_{visc} .

(iv) What is the influence of ambient gas on disc evolution? This broad topic includes a number of questions regarding both star formation physics and the response of the disc to the ISM. Some of these include: How long is the embedded phase as a function of environment? How efficient is extinction in regions of high gas density? What is the statistical influence of the motion of the dense ISM with respect to a population of PPDs? The first two of these questions can now be addressed systematically with high-resolution imaging of GMC population across the nearby galaxy population (Kruijssen et al. 2019; Chevance et al. 2019).

Overall, we conclude that building a picture of planet formation predominantly based on PPDs in the solar neighbourhood, or ignoring the dependence of their properties on host stellar mass or the galactic environment will result in a biased understanding of the time and mass available for planet formation over the galactic and cosmological scales relevant for studies of the exoplanet population. The prescription we have presented is a tool for future studies wishing to estimate the variation of PPD properties in diverse environments. Our findings highlight the key issues that need to be addressed in order to further establish the importance of star formation conditions for planet formation.

ACKNOWLEDGEMENTS

We thank the anonymous referee for a considerate report that improved the clarity of this manuscript. We thank Sebastian Trujillo-Gomez for kindly sharing his results, quantifying the minimum mass of a star forming region, prior to publication. AJW thanks Richard Booth and Cathie

Clarke for useful comments and discussion. AJW gratefully acknowledges funding from the European Research Council (ERC) under the European Union’s Horizon 2020 research and innovation programme (grant agreement No 681601). AJW gratefully acknowledges support from Sonderforschungsbereich SFB 881 “The Milky Way System” (subproject B2) of the German Research Foundation (DFG). JMDK and MC gratefully acknowledge funding from the DFG via an Emmy Noether Research Group (grant number KR4801/1-1). JMDK and BWK gratefully acknowledge from the European Research Council (ERC) under the European Union’s Horizon 2020 research and innovation programme via the ERC Starting Grant MUSTANG (grant agreement number 714907). BWK acknowledges funding in the form of a Postdoctoral Research Fellowship from the Alexander von Humboldt Stiftung.

REFERENCES

- Abadi M. G., Navarro J. F., Steinmetz M., Eke V. R., 2003, *ApJ*, 591, 499
- Adamo A., Kruijssen J. M. D., Bastian N., Silva-Villa E., Ryon J., 2015, *MNRAS*, 452, 246
- Adams F. C., 2010, *ARA&A*, 48, 47
- Agertz O., Kravtsov A. V., Leitner S. N., Gnedin N. Y., 2013, *ApJ*, 770, 25
- Ali A. A., Harries T. J., 2019, *MNRAS*, 487, 4890
- Anderson K. R., Adams F. C., Calvet N., 2013, *ApJ*, 774, 9
- Andrews S. M., Rosenfeld K. A., Kraus A. L., Wilner D. J., 2013, *ApJ*, 771, 129
- Ansdell M., Williams J. P., Manara C. F., Miotello A., Facchini S., van der Marel N., Testi L., van Dishoeck E. F., 2017, *AJ*, 153, 240
- Armitage P. J., 2000, *A&A*, 362, 968
- Barnes A. T., Longmore S. N., Battersby C., Bally J., Kruijssen J. M. D., Henshaw J. D., Walker D. L., 2017, *MNRAS*, 469, 2263
- Bate M. R., 2018, *MNRAS*, 475, 5618
- Baumgardt H., Kroupa P., 2007, *MNRAS*, 380, 1589
- Bertoldi F., McKee C. F., 1992, *ApJ*, 395, 140
- Binney J., Tremaine S., 1987, *Galactic dynamics*. Princeton University Press
- Bisbas T. G., et al., 2015, *MNRAS*, 453, 1324
- Bolatto A. D., Leroy A. K., Rosolowsky E., Walter F., Blitz L., 2008, *ApJ*, 686, 948
- Breslau A., Steinhausen M., Vincke K., Pfalzner S., 2014, *A&A*, 565, A130
- Bressert E., et al., 2010, *MNRAS*, 409, L54
- Burkert A., Hartmann L., 2004, *ApJ*, 616, 288
- Cardelli J. A., Clayton G. C., Mathis J. S., 1989, *ApJ*, 345, 245
- Castelli F., Kurucz R. L., 2004, *ArXiv Astrophysics e-prints*
- Chevance M., et al., 2019, *MNRAS* submitted
- Clarke C. J., 2007, *MNRAS*, 376, 1350
- Clarke C. J., Pringle J. E., 1993, *MNRAS*, 261, 190
- Clarke C. J., Gendrin A., Sotomayor M., 2001, *MNRAS*, 328, 485
- Clarkson W. I., Ghez A. M., Morris M. R., Lu J. R., Stolte A., McCrady N., Do T., Yelda S., 2012, *ApJ*, 751, 132
- Cleeves L. I., Öberg K. I., Wilner D. J., Huang J., Loomis R. A., Andrews S. M., Czekala I., 2016, *ApJ*, 832, 110
- Dib S., Bell E., Burkert A., 2006, *ApJ*, 638, 797
- Efstathiou G., 2000, *MNRAS*, 317, 697
- Elmegreen B. G., 2002, *ApJ*, 577, 206
- Elmegreen B. G., 2007, *ApJ*, 668, 1064
- Elmegreen B. G., Falgarone E., 1996, *ApJ*, 471, 816
- Evans II N. J., et al., 2009, *ApJS*, 181, 321

- Facchini S., Clarke C. J., Bisbas T. G., 2016, *MNRAS*, 457, 3593
- Fatuzzo M., Adams F. C., 2008, *ApJ*, 675, 1361
- Federrath C., Roman-Duval J., Klessen R. S., Schmidt W., Mac Low M.-M., 2010, *A&A*, 512, A81
- Figier D. F., McLean I. S., Morris M., 1999, *ApJ*, 514, 202
- Freeman P., Rosolowsky E., Kruijssen J. M. D., Bastian N., Adamo A., 2017, *MNRAS*, 468, 1769
- Ginsburg A., et al., 2018, *ApJ*, 853, 171
- Guesten R., Henkel C., 1983, *A&A*, 125, 136
- Habing H. J., 1968, *Bull. Astron. Inst. Netherlands*, 19, 421
- Haisch Jr. K. E., Lada E. A., Lada C. J., 2001, *ApJ*, 553, L153
- Hall S. M., Clarke C. J., Pringle J. E., 1996, *MNRAS*, 278, 303
- Haworth T. J., Facchini S., Clarke C. J., Cleeves L. I., 2017, *MNRAS*, 468, L108
- Haworth T. J., Facchini S., Clarke C. J., Mohanty S., 2018a, *MNRAS*, 475, 5460
- Haworth T. J., Clarke C. J., Rahman W., Winter A. J., Facchini S., 2018b, *MNRAS*, 481, 452
- Henshaw J. D., Longmore S. N., Kruijssen J. M. D., 2016, *MNRAS*, 463, L122
- Hernquist L., 1990, *ApJ*, 356, 359
- Heyer M., Krawczyk C., Duval J., Jackson J. M., 2009, *ApJ*, 699, 1092
- Hill T., et al., 2012, *A&A*, 542, A114
- Hirota A., et al., 2018, *PASJ*, 70, 73
- Hollenbach D. J., Tielens A. G. G. M., 1997, *ARA&A*, 35, 179
- Hollenbach D., Johnstone D., Lizano S., Shu F., 1994, *ApJ*, 428, 654
- Hopkins P. F., Quataert E., Murray N., 2012, *MNRAS*, 421, 3522
- Johansen A., Lambrechts M., 2017, *Annual Review of Earth and Planetary Sciences*, 45, 359
- Johnstone D., Hollenbach D., Bally J., 1998, *ApJ*, 499, 758
- Kennicutt Jr. R. C., 1989, *ApJ*, 344, 685
- Kroupa P., 2001, *MNRAS*, 322, 231
- Kruijssen J. M. D., 2012, *MNRAS*, 426, 3008
- Kruijssen J. M. D., 2015, *MNRAS*, 454, 1658
- Kruijssen J. M. D., Longmore S. N., 2013, *MNRAS*, 435, 2598
- Kruijssen J. M. D., Longmore S. N., Elmegreen B. G., Murray N., Bally J., Testi L., Kennicutt R. C., 2014, *MNRAS*, 440, 3370
- Kruijssen J. M. D., Dale J. E., Longmore S. N., 2015, *MNRAS*, 447, 1059
- Kruijssen J. M. D., et al., 2019, *Nature*, 569, 519
- Krumholz M. R., McKee C. F., 2005, *ApJ*, 630, 250
- Krumholz M. R., Tan J. C., 2007, *ApJ*, 654, 304
- Krumholz M. R., McKee C. F., Bland -Hawthorn J., 2019, *ARA&A*, 57, 227
- Kuffmeier M., Frimann S., Jensen S. S., Haugbølle T., 2018, *MNRAS*, 475, 2642
- Lada C. J., Lada E. A., 2003, *ARA&A*, 41, 57
- Leroy A. K., et al., 2017, *ApJ*, 846, 71
- Longmore S. N., et al., 2013, *MNRAS*, 429, 987
- Longmore S. N., et al., 2014, *Protostars and Planets VI*, pp 291–314
- Lynden-Bell D., Pringle J. E., 1974, *MNRAS*, 168, 603
- Mac Low M.-M., Ferrara A., 1999, *ApJ*, 513, 142
- Manara C. F., et al., 2016, *A&A*, 591, L3
- Martin C. L., Kennicutt Jr. R. C., 2001, *ApJ*, 555, 301
- Maschberger T., Clarke C. J., 2008, *MNRAS*, 391, 711
- Matzner C. D., McKee C. F., 2000, *ApJ*, 545, 364
- McKee C. F., Ostriker J. P., 1977, *ApJ*, 218, 148
- Mengel S., Tacconi-Garman L. E., 2007, *A&A*, 466, 151
- Merín B., et al., 2008, *ApJS*, 177, 551
- Moeckel N., Throop H. B., 2009, *ApJ*, 707, 268
- Molinari S., et al., 2014, *Protostars and Planets VI*, pp 125–148
- Muñoz D. J., Kratter K., Vogelsberger M., Hernquist L., Springel V., 2015, *MNRAS*, 446, 2010
- Nakajima Y., Tamura M., Oasa Y., Nakajima T., 2000, *AJ*, 119, 873
- Olczak C., Pflanzner S., Spurzem R., 2006, *ApJ*, 642, 1140
- Olczak C., Kaczmarek T., Harfst S., Pflanzner S., Portegies Zwart S., 2012, *ApJ*, 756, 123
- Ormel C. W., Liu B., Schoonenberg D., 2017, *A&A*, 604, A1
- Ostriker E. C., 1994, *ApJ*, 424, 292
- Padoan P., Nordlund Å., 2002, *ApJ*, 576, 870
- Padoan P., Nordlund Å., 2011, *ApJ*, 730, 40
- Padoan P., Nordlund A., Jones B. J. T., 1997, *MNRAS*, 288, 145
- Pascucci I., et al., 2016, *ApJ*, 831, 125
- Pflanzner S., Vogel P., Scharwächter J., Olczak C., 2005a, *A&A*, 437, 967
- Pflanzner S., Umbreit S., Henning T., 2005b, *ApJ*, 629, 526
- Pflanzner S., Olczak C., Eckart A., 2006, *A&A*, 454, 811
- Predehl P., Schmitt J. H. M. M., 1995, *A&A*, 293, 889
- Rathborne J. M., et al., 2014, *ApJ*, 795, L25
- Reina-Campos M., Kruijssen J. M. D., 2017, *MNRAS*, 469, 1282
- Ribas Á., Merín B., Bouy H., Maud L. T., 2014, *A&A*, 561, A54
- Rosolowsky E., Blitz L., 2005, *ApJ*, 623, 826
- Rosotti G. P., Dale J. E., de Juan Ovelar M., Hubber D. A., Kruijssen J. M. D., Ercolano B., Walch S., 2014, *MNRAS*, 441, 2094
- Rosotti G. P., Clarke C. J., Manara C. F., Facchini S., 2017, *MNRAS*, 468, 1631
- Schaller G., Schaerer D., Meynet G., Maeder A., 1992, *A&AS*, 96, 269
- Schechter P., 1976, *ApJ*, 203, 297
- Scicluna P., Rosotti G., Dale J. E., Testi L., 2014, *A&A*, 566, L3
- Shakura N. I., Sunyaev R. A., 1973, *A&A*, 24, 337
- Silk J., 1997, *ApJ*, 481, 703
- Spitzer L., 1978, *Physical processes in the interstellar medium*. New York Wiley-Interscience, 1978. 333 p., doi:10.1002/9783527617722
- Stolte A., et al., 2010, *ApJ*, 718, 810
- Stolte A., et al., 2014, *ApJ*, 789, 115
- Stolte A., et al., 2015, *A&A*, 578, A4
- Störzer H., Hollenbach D., 1999, *ApJ*, 515, 669
- Strömgren B., 1939, *ApJ*, 89, 526
- Sun J., et al., 2018, *ApJ*, 860, 172
- Tielens A. G. G. M., Hollenbach D., 1985, *ApJ*, 291, 722
- Toomre A., 1964, *ApJ*, 139, 1217
- Trujillo-Gomez S., Reina-Campos M., Kruijssen J. M. D., 2019, *MNRAS*, 488, 3972
- Utomo D., et al., 2018, *ApJ*, 861, L18
- Vazquez-Semadeni E., 1994, *ApJ*, 423, 681
- Vincke K., Pflanzner S., 2018, *ApJ*, 868, 1
- Wijnen T. P. G., Pols O. R., Pelupessy F. I., Portegies Zwart S., 2017a, *A&A*, 602, A52
- Wijnen T. P. G., Pols O. R., Pelupessy F. I., Portegies Zwart S., 2017b, *A&A*, 604, A91
- Winter A. J., Clarke C. J., Rosotti G., Booth R. A., 2018a, *MNRAS*, 475, 2314
- Winter A. J., Clarke C. J., Rosotti G., Ih J., Facchini S., Haworth T. J., 2018b, *MNRAS*, 478, 2700
- Winter A. J., Booth R. A., Clarke C. J., 2018c, *MNRAS*, 479, 5522
- Winter A. J., Clarke C. J., Rosotti G. P., Hacer A., Alexander R., 2019a, arXiv e-prints, p. arXiv:1909.04093
- Winter A. J., Clarke C. J., Rosotti G. P., 2019b, *MNRAS*, 485, 1489
- Wong T., Blitz L., 2002, *ApJ*, 569, 157
- Youdin A. N., Goodman J., 2005, *ApJ*, 620, 459
- de Juan Ovelar M., Kruijssen J. M. D., Bressert E., Testi L., Bastian N., Cánovas H., 2012, *A&A*, 546, L1

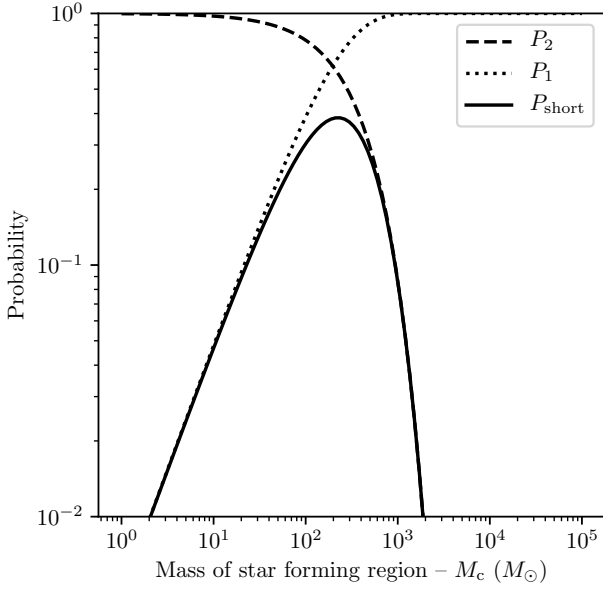


Figure A1. Probability, P_1 , of a star with a short lifetime ($\lesssim 10$ Myr – dotted line) and the probability P_2 , of no star in the range $12\text{--}16 M_\odot$ occupying a star forming region of mass M_c (dashed line). The product of these two probabilities P_{short} is the probability of a star forming environment being strongly irradiated for a period < 10 Myr (equation A2 – solid line).

APPENDIX A: SHORT-LIVED FUV IRRADIATION

We have assumed in our models that massive stars in a given star forming region do not reach the end of their lifetime before PPDs are dispersed. In this appendix we explore this assumption. The main sequence lifetime of stars can be approximated:

$$\frac{\tau_{\text{MS}}}{10^4 \text{ Myr}} \sim \left(\frac{m_*}{M_\odot} \right)^{-2.5}.$$

For the strongest FUV environments where $\tau_{\text{FUV}} \lesssim 1$ Myr, our approximation is reasonable since even the most massive stars survive over this time-scale. For stars of stellar mass $m_* \gtrsim 12 M_\odot \equiv M_{\text{FUV}}$, the FUV luminosity is within approximately an order of magnitude of the most massive stars (e.g. Winter et al. 2018b). For stellar masses $m_* \gtrsim 16 M_\odot \equiv M_{\text{short}}$, $\tau_{\text{MS}} \lesssim 10$ Myr.

To approximate the frequency of systems where PPDs can be strongly irradiated for short periods, we estimate the probability P_{short} that a short-lived star with $m_* > M_{\text{short}}$ exists in a star forming region (with probability P_1), but there is no star with a mass in the range $M_{\text{FUV}} < m_* < M_{\text{short}}$ (with probability P_2). If the latter condition is not met, then even when the most massive star in the region reaches the end of its lifetime, then the drop in the FUV luminosity of the most massive remaining star will be less than an order of magnitude. The fraction of stars between masses M_1 and M_2 is:

$$\Xi_{M_1}^{M_2} = \int_{M_1}^{M_2} \xi_* dm_* \quad (\text{A1})$$

where ξ_* is the normalised IMF (equation 6). Then we have:

$$P_{\text{short}} = \underbrace{\left[1 - \left(1 - \Xi_{M_{\text{short}}}^\infty \right)^{N_c} \right]}_{P_1} \cdot \underbrace{\left(1 - \Xi_{M_{\text{FUV}}}^{M_{\text{short}}} \right)^{N_c}}_{P_2} \quad (\text{A2})$$

where the number of stars N_* in the star forming region is $N_c = M_c / \langle m_* \rangle \approx M_c / 0.5 M_\odot$.

The result of the calculation of P_1 and P_2 as a function of the stellar mass of the star forming region is shown in Figure A1. In the range $\sim 30\text{--}1000 M_\odot$, where P_{short} is maximised, we find that there is a 10–40 percent chance of a short lived period of strong exposure to FUV flux. This possibility warrants further exploration in future investigations, however we do not do so here. We justify our simplification in that the regions of the highest FUV flux exhibit disc lifetimes $\ll 10$ Myr, so our estimates in this section are an upper limit on the significance of short main sequence lifetimes.

APPENDIX B: FUV EXTINCTION

B1 Modified flux distribution

At early times, the presence of ambient gas causes intra-cluster extinction in the FUV; we wish to evaluate its influence on the flux PDF at fixed x . This is dependent on the effective local gas surface density Σ_{eff} between a given star and FUV source. We define the corresponding surface overdensity $\chi \equiv \Sigma_{\text{eff}} / \Sigma_0$. In order to proceed, we assume that the local extinction does not influence the flux in the field, which remains the floor of the distribution of F . Then the ratio of the extincted flux to the local mean flux is $\psi_0^{\text{ext}} \equiv F_0^{\text{ext}} / F_0^{\text{HM}}$ is

$$\psi_0^{\text{ext}} = e^{-C_{\text{ext}} \chi} \Lambda + \psi_0^{\text{f}}. \quad (\text{B1})$$

As before, we can immediately evaluate the PDF for ψ_0^{ext} at certain limits. Equation 59 applies here as before, as does equation 60. However, ψ_0^{ext} is now determined by χ as well as x and Λ . We must therefore evaluate the PDF for χ .

B2 Effective surface density

B2.1 Gas density profile

To evaluate the appropriate surface density, we are required to make assumptions about the geometry of the system. This involves introducing an additional parameter, describing the relative position in a local environment such that we can link ρ_g to Σ_{eff} . We define a radial coordinate r within a star-forming region of scale radius a , and the relative radius $\gamma \equiv r/a$. Fatuzzo & Adams (2008) define a Hernquist (1990) density profile to calculate the apparent surface density. However, this form implies an infinite central density, which is inconsistent with our assumption that gas density is lognormally distributed. We instead choose a Plummer density profile:

$$\rho_g = \frac{\rho_c}{(1 + \gamma^2)^{5/2}}. \quad (\text{B2})$$

The local overdensity in the centre $x_c \equiv \rho_c / \rho_0$ is a bijective function of $\gamma > 0$ for $x < x_c$, and we assume the same

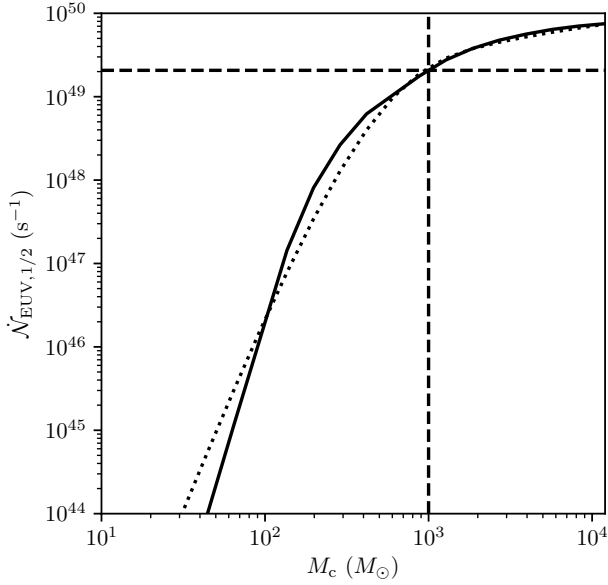


Figure B1. As in Figure 3 but for the number of EUV counts $\dot{N}_{\text{EUV},1/2}$. The solid line is calculated directly from random drawing and the stellar atmosphere models used in this work, while the dotted line follows our analytic approximation, equation B6. The vertical dashed line is at M_{crit} and the corresponding number of counts $\dot{N}_{\text{EUV,crit}} = 2.07 \times 10^{49} \text{ s}^{-1}$ is shown as a horizontal dashed line.

lognormal PDF as for x truncated below this value. The corresponding PDF for γ at fixed x is

$$\frac{\partial \mathcal{F}_*}{\partial \gamma} = \frac{\partial \mathcal{F}_*}{\partial x_c} \frac{\partial x_c}{\partial \gamma} \propto \gamma (1 + \gamma^2)^4 \frac{\partial p}{\partial x_c}, \quad (\text{B3})$$

where $\partial p / \partial x_c \propto \partial p / \partial x$ for $x < x_c$ and vanishes otherwise. As a sanity check, we consider the functional dependence on the distribution of γ for small and large x . Since the over-density PDF is lognormal, for large x then as x increases the (negative) slope of the PDF for x_c also increases. Therefore, at large x we preferentially find small γ . This is exactly what we would expect since extremely high densities should be rare at large radii. Similarly, for small x a large value of γ is favoured. For a given γ , we can also calculate the corresponding a such that the total gas mass is $\phi M_{\text{crit}} / \epsilon$:

$$a = \left(\frac{3M_{\text{crit}}}{4\pi\epsilon\rho_0 x_c} \right)^{1/3} = \left(\frac{3M_{\text{crit}}}{4\pi\epsilon\rho_0} \right)^{1/3} x^{-1/3} \phi^{1/3} (1 + \gamma^2)^{-5/6}. \quad (\text{B4})$$

Thus we define a density profile that is self-consistent with a given x , ϕ .

B2.2 Ionisation

Having defined our local density profile, we integrate over the relevant range to establish the effective surface density. When a massive star occupies the central region of a given environment then we would expect material within a certain radius to be ionised (and therefore optically thin to FUV photons). This size scale is initially given by the [Strömgren](#)

(1939) radius:

$$R_S \approx \left(\frac{3\dot{N}_{\text{LyC}} m_p^2}{4\pi\alpha_B \rho_c^2} \right)^{1/3} = \left(\frac{3\dot{N}_{\text{LyC}} m_p^2}{4\pi\alpha_B \rho_0^2} \right)^{1/3} x^{-2/3} (1 + \gamma^2)^{-5/3} \quad (\text{B5})$$

where \dot{N}_{LyC} is the number of ionising (Lyman continuum) photons emitted by the central source per unit time, $\alpha_B \approx 2.7 \times 10^{-13} \text{ cm}^3 \text{ s}^{-1}$ is the recombination coefficient assuming a temperature $\sim 10^4 \text{ K}$ for the ionised gas. For convenience we have approximated a constant local density for $r < R_S$, which holds for if $R_S \lesssim a$. This is true for large x , where we will find that extinction is significant.

We assume EUV photons dominate ionisation and define the median number of EUV counts from the most massive star $\dot{N}_{\text{EUV},1/2}(\phi)$. For this we define a fitting formula:

$$\Theta(\phi) \equiv \frac{\dot{N}_{\text{EUV},1/2}}{\dot{N}_{\text{EUV,crit}}} \approx \left\{ 1 - e^{-\delta_1 \phi} \right\}^{\delta_2} \ln(1 + \delta_1 \phi) \quad (\text{B6})$$

where $\dot{N}_{\text{EUV,crit}} = 2.07 \times 10^{49} \text{ s}^{-1}$, and we find $\delta_1 = 2.9$, $\delta_2 = 4.0$. This expression is compared to the direct calculation from the adopted stellar atmosphere models in Figure B1.

Combining equations B5 and B6, we have:

$$\gamma_S \equiv \frac{R_S}{a} = \left(\frac{\dot{N}_{\text{EUV,crit}} m_p^2}{\alpha_B M_{\text{crit}} \rho_0} \right)^{1/3} \epsilon^{1/3} x^{-1/3} \phi^{-1/3} (1 + \gamma^2)^{-5/6} \Theta^{1/3}, \quad (\text{B7})$$

in dimensionless quantities. Evaluating the prefactor yields:

$$\left(\frac{\dot{N}_{\text{EUV,crit}} m_p^2}{\alpha_B M_{\text{crit}} \rho_0} \right)^{1/3} \approx \left(\frac{\rho_0}{1.6 M_\odot \text{ pc}^{-3}} \right)^{-1/3}. \quad (\text{B8})$$

B2.3 Effective surface density PDF outside Strömgren radius

We assume that F is dominated by sources at the center of the density profile. Assuming spherical geometry, then the effective surface density is that of a spherical shell and we have:

$$\Sigma_{\text{eff}} = a \int_{\gamma_S}^{\gamma} \frac{(1 - \epsilon)\rho_c}{(1 + \tilde{\gamma}^2)^{5/2}} d\tilde{\gamma} \quad (\text{B9})$$

By making the simplifying assumption that the SFE is approximately constant over the region such that $\epsilon = \epsilon(x) \neq \epsilon(\gamma)$, we can evaluate equation B9 in terms of dimensionless parameters:

$$\chi_1 \approx \frac{(1 - \epsilon)}{3\epsilon^{1/3}} \left(\frac{3M_{\text{crit}} \rho_0^2}{4\pi\Sigma_0^3} \right)^{1/3} x^{2/3} \phi^{1/3} (1 + \gamma)^{5/3} \times \left\{ \frac{\gamma(2\gamma^2 + 3)}{(1 + \gamma^2)^{3/2}} - \frac{\gamma_S(2\gamma_S^2 + 3)}{(1 + \gamma_S^2)^{3/2}} \right\}, \quad (\text{B10})$$

where we have defined $\chi_1 \equiv \chi(\gamma > \gamma_S)$, since $\chi(\gamma < \gamma_S) = 0$.

Now we have a definition for χ , we can use the PDF for γ (equation B3) and ϕ (equation 62) to calculate the corresponding PDF for χ at a fixed x . However, since there is a non-zero probability that $\chi = 0$, we must separately consider the regions inside and outside the Strömgren radius.

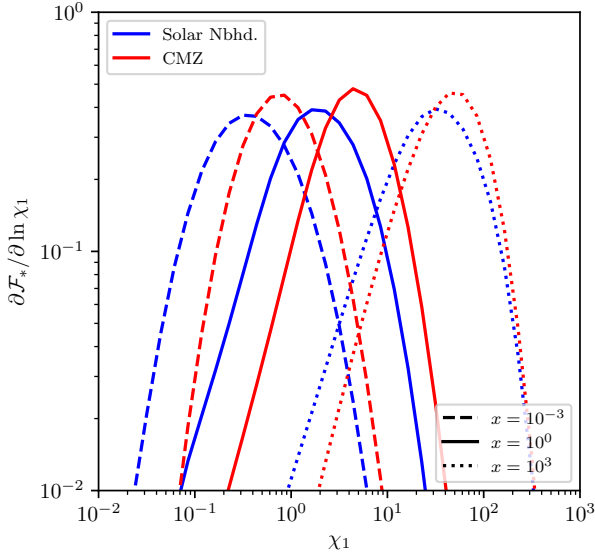


Figure B2. PDF of χ_1 (i.e. χ such that we assume $\chi > 0$) for varying overdensity x in the solar neighbourhood (blue lines) and CMZ (red lines). The value of χ_1 is the normalised effective surface density experienced by a given star in the direction of the centre of the star-forming region during the embedded phase.

We first evaluate the PDF of χ_1 (that is, assuming $\chi > 0$ – a star outside the Strömgren radius):

$$\frac{\partial \mathcal{F}_*}{\partial \chi_1} = \int d\phi \frac{\partial \mathcal{F}_*}{\partial \phi} \frac{\partial \mathcal{F}_*}{\partial \gamma} \left| \frac{\partial \chi_1}{\partial \gamma} \right|^{-1}, \quad (\text{B11})$$

Here it is necessary to evaluate $\gamma(\phi, \chi_1)$ numerically. The result is shown in Figure B2 for solar neighbourhood- and CMZ-like regions. We find that the effective surface density experienced by a given star increases with local gas density x , as expected. We therefore expect regions of high overdensity to be severely influenced by extinction. However, we must also consider the fact that stars at high density are more likely to be found towards the centre of the region, and therefore to occupy the Strömgren sphere (hence $\chi = 0$). It is necessary to explore the possibility that this influences our results.

B2.4 Fraction of stars born within the Strömgren radius

The probability that $\chi = 0$ is equivalent to the probability that a star is found inside a radius γ_S . This can be written:

$$p_S(\phi, x) \equiv \mathcal{F}_*(\chi = 0; \phi, x) = \int_{\gamma < \gamma_S} d\gamma \frac{\partial \mathcal{F}_*}{\partial \gamma}, \quad (\text{B12})$$

where the region $\gamma < \gamma_S$ is defined numerically for a fixed ϕ , x . Equation B12 is evaluated in Figure B3, from which we find that the probability of finding a star within a Strömgren radius is small ($\ll 10\%$) throughout the parameter space, especially for high ρ_0 environments. This is intuitively true from equation B7; in the limit of large ρ_0 , x , ϕ , we have small γ_S , and hence a small p_S . Since the contribution to the PDF from stars with $\gamma < \gamma_S$ is small, we have $\partial \mathcal{F}_*/\partial \chi_1 \approx \partial \mathcal{F}_*/\partial \chi$ and we are free to limit our consideration to the distribution of $\chi_1 > 0$ in calculation of the PDF for ψ_0^{ext} . While we are here interested in initial conditions, it should also be noted

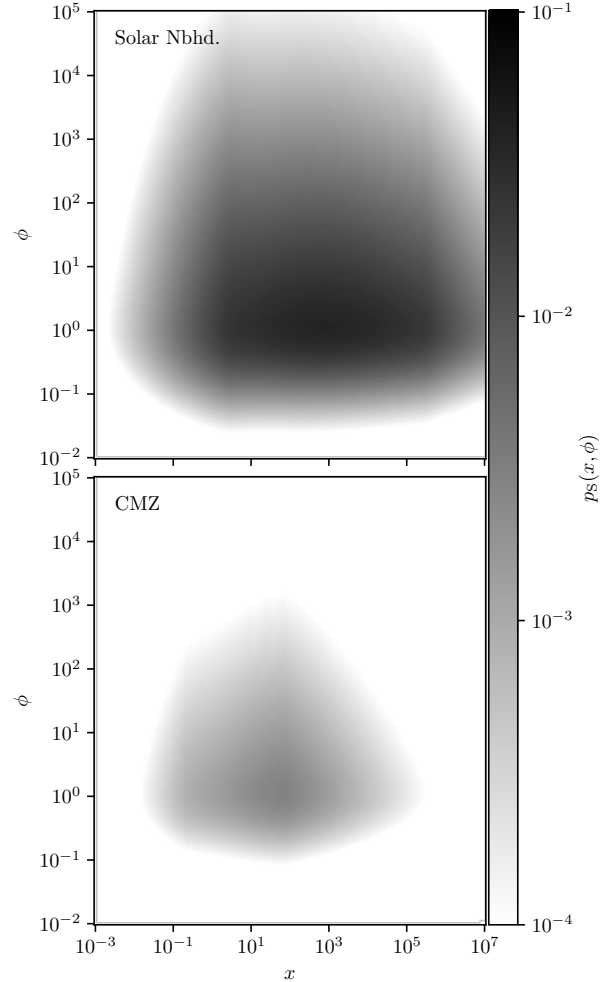


Figure B3. Probability p_S of finding a given star within the Strömgren radius ($\gamma < \gamma_S$) as a function of the stellar mass ϕ of the star-forming region and overdensity x for the solar neighbourhood (top panel) and CMZ (bottom panel). This is equivalent to the probability that a star has $\chi = 0$, and does not experience significant extinction of FUV photons from neighbouring stars.

that physically this radius expands over time (see Section B3 below).

B3 PDF for extincted FUV flux

As a result of the above analysis, we can now simply write the PDF for ψ_0^{ext} :

$$\frac{\partial \mathcal{F}_*}{\partial \psi_0^{\text{ext}}} \approx \int_{\delta\chi}^{\infty} d\chi_1 \frac{\partial \mathcal{F}_*}{\partial \chi_1} \frac{\partial \mathcal{F}_*}{\partial \phi} \left| \frac{\partial \psi_0^{\text{ext}}}{\partial \phi} \right|^{-1} \quad (\text{B13})$$

for some sufficiently small $\delta\chi$. Equation B13 is the PDF for the flux in the embedded phase of the cluster or association (at fixed x), and can be compared to the non-extincted PDF (equation 61) to estimate the role of gas with regards to stellar birth environment at early times.

We stress that this formulation gives an upper limit to the extinction experienced within a given environment. We have neglected the fact that realistically we would expect a clumpy density distribution, which can considerably reduce

the influence of extinction ([Ali & Harries 2019](#)). Additionally, we have established the Strömgren radius by assuming a constant central density, and the EUV luminosity of the single most massive star. In the case of a steep density profile, or multiple ionising sources, this will be an underestimate. Nor have we considered the rate of expansion of such an ionised region over time t ; physically the radius of the ionised region scales with $(c_{\text{st}}/R_{\text{S}})^{4/7}$ (e.g. [Spitzer 1978](#); [Bisbas et al. 2015](#)). For these reasons, the true FUV flux experienced by a star is likely to be larger than the estimate we establish here.

This paper has been typeset from a $\text{\TeX}/\text{\LaTeX}$ file prepared by the author.